Review Paper

Metal oxide nanoparticles and their applications in nanotechnology

Murthy S. Chavali[1] · **Maria P. Nikolova**[2]

Abstract

Considering metal oxide nanoparticles as important technological materials, authors provide a comprehensive review of researches on metal oxide nanoparticles, their synthetic strategies, and techniques, nanoscale physicochemical properties, defining specific industrial applications in the various fields of applied nanotechnology. This work expansively reviews the recent developments of semiconducting metal oxide gas sensors for environmental gases including CO_2, O_2, O_3, and NH_3; highly toxic gases including CO, H_2S, and NO_2; combustible gases such as CH_4, H_2, and liquefied petroleum gas; and volatile organic compounds gases. The gas sensing properties of different metal oxides nanoparticles towards specific target gases have been individually discussed. Promising metal oxide nanoparticles for sensitive and selective detection of each gas have been identified. This review also categorizes metal oxides sensors by analyte gas and also summarizes the major techniques and synthesis strategies used in nanotechnology. Additionally, strategies, sensing mechanisms and related applications of semiconducting metal oxide materials are also discussed in detail. Related applications are innumerable trace to ultratrace-level gas sensors, batteries, magnetic storage media, various types of solar cells, metal oxide nanoparticles applications in catalysis, energy conversion, and antennas (including microstrip and patch-type optically transparent antennas), rectifiers, optoelectronic, and electronics.

Keywords Metal oxide · MONPs · Gas sensors · Batteries · Antennas · Solar cells · Optoelectronics

Abbreviations

1D	One-dimensional
3D	Three-dimensional
Ag	Silver
AgHT film	Silver-coated polyester film
ALD	Atomic layer deposition
ANSYS	Analysis systems
Ar	Argon
Au	Gold
BPE	Bulk photovoltaic effect
CH_4	Methane
CNTs	Carbon nanotubes
CO	Carbon monoxide
Co	Cobalt
CO_2	Carbon dioxide
Cr	Chromium
CVD	Chemical vapour deposition
DC sputtering	Direct current sputtering
DSCs	Dye solar cells
DSSC	Dye-sensitized solar cell (Grätzel cell)
EBL	Electron beam lithography
EM	Electromagnetic
GHz	Gigahertz
GO	Graphene oxide
GPS	Global positioning system
H_2	Hydrogen
H_2S	Hydrogen sulphide
HF	High frequency
HFSS	High-frequency electromagnetic field simulation
HPHT	High pressure/high temperature
IC	Internal combustion
IC_{50}	Half-maximal inhibitory concentration
II	Ion implantation

✉ Maria P. Nikolova, mpnikolova@uni-ruse.bg | [1]Shree Velagapudi Ramakrishna Memorial College (SVRMC-PG Studies), NAAC 'A' Grade and ISO 9001:2015 Certified, (Autonomous), Nagaram and MCETRC, Tenali, Guntur District, Andhra Pradesh 522201, India. [2]Department of Material Science and Technology, University of Ruse "A. Kanchev", 8 Studentska Str, 7017 Ruse, Bulgaria.

SN Applied Sciences (2019) 1:607 | https://doi.org/10.1007/s42452-019-0592-3

Received: 22 February 2019 / Accepted: 10 May 2019 / Published online: 20 May 2019

IMT	Insulator–metal transition
IR	Infrared
ITO	Indium tin oxide
IZO	Indium zinc oxide
LCDs	Liquid crystal displays
LED	Light-emitting diode
Li	Lithium
LIBs	Lithium-ion batteries
LLNL	Lawrence Livermore National Laboratory
MBE	Molecular beam epitaxy
MIM	Metal–insulator–metal
MO	Metal oxide
MOC	Multivariate optical computing
MOE	Multivariate optical element
MONPs	Metal oxides nanoparticles
MOS	Metal oxide semiconductors
MO_x	Nanosized metal oxides
MPA	Microstrip patch antenna
MRI	Magnetic resonance imaging
MSD	Magnetic storage devices
NH_3	Ammonia
nm	Nanometer
NO	Nitrogen monoxide
NO_2	Nitrogen dioxide
NP	Nanoparticle
O_2	Oxygen
O_3	Ozone
OLED	Organic light-emitting diode
OP	Optically transparent
PCBs	Printed circuit boards
PCE	Power conversion efficiency
pH	Power of hydrogen
PLD	Pulsed laser deposition
PM	Particulate matter
ppb	Parts per billion
ppm	Parts per million
Pt	Platinum
p-TCO	*p*-type transparent conducting oxide
PV	Photovoltaics
PVD	Pulse vapour deposition
PZT	Lead zirconate titanate
QDs	Quantum dots
RF Sputtering	Radio-frequency sputtering
RFID	Radio-frequency identification
rGO	Reduced graphene oxide
RGTO	Rheotaxial growth and thermal oxidation
RH	Relative humidity
RMS	Reactive magnetron sputtering
RT	Room temperature
SIBs	Sodium-ion batteries
SP	Spray pyrolysis
SWCNT	Single-walled carbon nanotube
TCM	Transparent conducting material
TCO	Transparent conducting oxide
TF	Thin film
THz	Terahertz
TMOs	Transition metal oxides
U mL^{-1}	Units per millilitre
UHF	Ultrahigh frequency
UV	Ultraviolet
VdW	Van der Waals
YSZ	Yttria-stabilized zirconia

1 Introduction

Semiconducting metal oxide-based gas sensors have attracted great attention for its advantages such as fast and sensitive detection portability and low cost, compared to other conventional techniques since their discovery of gas sensing properties in 1960s. The engineered metal oxides nanoparticles (MONPs) are among the widest used manufactured nanomaterials because of their unique properties. The properties that make the nanophase structures indispensable tools in modern nanotechnology are their various nonlinear optical properties, higher ductility at elevated temperatures than the coarse-grained ceramics, cold welding properties, superparamagnetic behaviour, unique catalytic, sensitivity, and selective activity. For example, the melting point of the nanosized material is lower than that of a bulk material with the same composition [1]. At the same time, NPs exhibit unusual adsorptive properties and fast diffusivities and they are not stable in critical conditions [2]. Nanotechnology includes the research and engineering of new materials at the nanoscale level. Several synthetic strategies and techniques were used in nanotechnology. As synthetic strategies are concerned, there are in general two types of approaches for the production of nanomaterials and fabrication of nanostructures.

(a) A bottom-up approach that includes miniaturization of materials components up to atomic level with further self-assembly process (physical forces operating at the nanoscale are used to combine basic units into larger stable structures) leading to the formation of nanostructures. This approach organizes atomic or molecular components in hierarchical nanocomplexes. Such examples are QDs or nanoparticles formed from colloidal dispersion;
(b) Top-down approach rather initiate with macroscopic structures, controlling externally the process of formation of nanostructures. The top-down approach

adds or removes thin layers of bulk materials as do ball milling, mask etching, etc.

Figure 1 summarizes the major techniques and synthesis strategies used in nanotechnology. The bottom-up approach for synthesis of nanostructured materials includes physical such as pulse and physical vapour deposition (PVD), chemical vapour deposition (CVD), pulsed laser deposition (PLD), ion implantation (II), atomic layer deposition (ALD), molecular beam epitaxy (MBE), spray pyrolysis (SP), and chemical methods for preparing NPs by an aqueous solution such as hydrothermal, precipitation and microemulsion routes, sol–gel, microwaved, sono-chemical electrochemical and photochemical processes [3, 4]. These physical and chemical production methods are typically pricey, labour-intensive and also detrimental to the environment [5].

Recently, a strong focus is placed on green synthesis, where NPs are extracted from fungi, algae, bacteria, and plants (usually terrestrial) in which a variety of metabolites

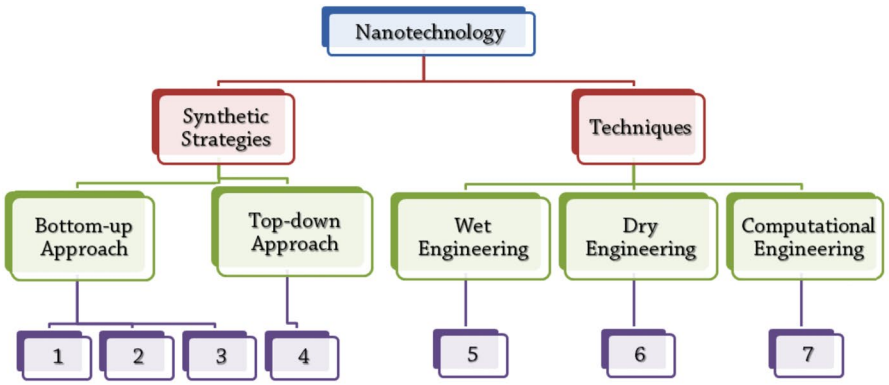

1	2	3	4
Physical *(Gas solid transformation)*	**Chemical** *(Liquid solid transformation)*	**Biological** *(Bioreduction)*	1. Bulk nanomachining 2. Fragmentation: Nanomilling, spark erosion, etc. 3. Lithography (Optical, ultraviolet, X-ray, electron beam, laser, etc.)
1. CVD and PVD 2. MBE 3. PLD 4. ALD 5. Ion-implantation 6. Spray pyrolysis	1. Co-precipitation 2. Sol-gel 3. Chemical reduction 4. Sono- and photochemical 5. Electrochemical 6. Microemulsion 7. Solvo-thermal (hydrothermal) 8. Template/surface derived method	1. By plants 2. By bacteria 3. By fungi 4. By yeast 5. By algae 6. By biomolecules 7. By agricultural and industrial wastes	

5	6	7
1. Biomimetic and tissue nanotechnology 2. Bioimaging, biosensing and bioanalytics 3. Nanodiagnostics 4. Nanotherapy 5. Pharmaceuticals 6. Cosmetics 7. Environment harvesting and remediation	1. Information processing, storage and transmission 2. Electronics, optoelectronics and photonics 3. Sensors, MEMs and energy devices 4. Food packaging and storage 5. Pigments, protective glasses, textiles	1. Ab-initio and semi empirical: a. Quantum or molecular mechanics b. Quantum or molecular dynamics of: *i. Nanostructures and interfaces* *ii. Assembly and growth* *iii. Biointeractions* 2. Optimisation and predictability

Fig. 1 Synthetic strategies and techniques used in nanotechnology, enlisting the typical processes or applications that a certain strategy or technique includes

act as reducing agents in NPs synthesis. The advantage of using green synthesis is that they are easily available, safe, and versatile in the type of metabolites that could act as reducing and stabilizing agents. Additionally, different combinations such as plant extracting with the microwave irradiation method that heats the material through its dielectric loss are recently proposed [6]. The obvious increase in the alternatives for the synthesis of NPs and green approaches that use different biological materials is greatly encouraging.

The nanotechnology techniques could be segregated into wet, dry, and computational engineering. Wet nanotechnology deals with the processes taking place in aqua-environments mostly exploiting living systems and components present in the cell, tissue, and organs of living organisms. Dry engineering handles synthesis of inorganic rigid structures and parts with the help of physicochemical methods, whereas computational nanotechnology concerns with the development and use of computer-based quantum and molecular design, modelling, and simulation of the behaviour or properties of systems relevant to nanotechnology.

The variety of methods employed during the fabrication of MONPs can alter the characteristics and control the properties of the obtained nano-oxides. The reaction mechanisms and, therefore, the functionality of nanostructured MO_x depend on their composition, crystallographic structure, morphology, surface stoichiometry and geometry, interactions of the phases, etc. For achieving nanostructures with a set of desired properties, it is vital to summarize the existing information for variations in functional properties and characteristics of nanostructured MO_x to expand our understanding beyond the existing knowledge. For that reason, this work was aimed at exploring the complications to induce further investigations by summarizing new techniques, benefitting the features of the MONPs and successful studies. The authors present various gas sensors, battery materials, solar cell, antennas, optoelectronic/electronic applications, etc., based on semiconducting MONPs and their composites used in nanotechnology. The many varieties of techniques, types of nano-oxides, and combinations used just confirm the complexity of correlation between changes of nanostructure and composition on the one hand, and on the other hand—the resultant properties of the designed device.

2 Properties of nano-oxides

At present, nanoparticle research is an area of intense scientific activity due to a variety of potential applications in several fields [7]. The electronic structure of nanoparticles can reveal semiconductor, metallic, or insulator character. The unique chemical and physical properties of MONPs are attributed to the high density and limited size of corners and edges on their surface. Potential technological applications of metal oxide nanoparticles play a vital role attracting researchers with considerable interest from the fields of materials chemistry, medicine, agriculture, information technology, biomedical, optical, electronics, catalysis, environment, energy, and sense. Changes in cell parameters due to the size-related structural alterations have been observed, for example, in nanoparticles of CuO, ZnO, SnO_2, Al_2O_3, MgO, ZrO_2 AgO, TiO_2, CeO_2, etc. As the size decreases in the nanoparticles, an increasing number of surface and interface atoms generates strain or stress and adjoining structural perturbations [8]. The specific size of the nanoparticle can alter magnetic, conducting, chemical, and electronic properties [9]. Magnetic metal oxides nanoparticles have gained particular interest as their properties can be tuned based on their size and shape. Magnetic, electronic, and chemical properties of nanoparticles can be dependent on a specific size of the nanoparticle material [10]. Iron oxides, precisely magnetite, are of particular interest to materials scientists as they are connected through series of potential applications, extending from magnetic storage devices (MSD) to magnetic resonance imaging (MRI) contrast agents [11]. Size-dependency was detected in γ-Fe_2O_3 nanoparticles, where 55 nm particles exhibit ferromagnetic behaviour, while 12 nm nanoparticles exhibit superparamagnetic behaviour without hysteresis [12]. The decrease in particle size will also decrease the total magnetic anisotropy while inducing the change to superparamagnetic [13]. Innovative easy methods of creating required sized metal oxide nanoparticles are essential for attaining all the desired magnetic, electronic, and chemical properties.

Electrical properties (conductance) are strongly dependant on the size of these particles especially using oxides like SnO_2, WO_3, and In_2O_3 [14] in gas sensing applications. Electrical/ionic conductivity is a property of TiO_2 materials that modulates to find practicality in the area of sensors, optoelectronics, or photovoltaics. TiO_2 can be easily reduced at high temperatures, and this assertively impacts conductivity [15]. One-dimensional (1-D) ZnO engaged in both optoelectronic and electronic applications [16] with wurtzite-type structure has tremendous potential in applications from gas sensors to varistors. The long-range effects of the Madelung field, present in the electronic properties of a bulk oxide surface, are either limited or not present in the nanostructured oxide [17].

Germania (GeO_2) nanoparticles have many prospective applications for enhancing optical fibres and other optoelectronic fields [18]. Ga_2O_3 nanoparticles are also used in surface-catalysed systems for new electronic or optical applications [19] specifically at low temperatures. As

a material with wider bandgap, it provides a broad range of light emission; β-Ga_2O_3 is presently being investigated to exploit its potential for optoelectronic applications. As known, the reduced-size nanoparticle enhances the chemical reactivity due to its larger surface area to unit mass ratio. The CuO nanoparticles are used in the microwave irradiation process, also as redox catalyst as well as a catalyst in several oxidation processes, in photoconductive and photothermal applications [20]. MgO nanoparticles are extensively applied in various types of chemical industries as a material for scrubber in eliminating gaseous air pollutants (CO_2, CO, NO_x, SO_x) and also as a catalyst in organic synthesis [21]. The novel structure of Al_2O_3 is used as a support for active phases in the area of catalysis coated with other materials [22]. ZrO_2 nanoparticles are exploited in structural ceramics, as a solid electrolyte, as a catalyst, and also as gas sensing materials [23]. CeO_2 nanoparticles are used in areas of catalysis, gas sensing, electrochemistry, biomedical, and material chemistry [24]. TiO_2 nanoparticles are applied in various kinds of industrial applications related to photocatalysis for pollutant elimination, solar cells, and also in material science and engineering [25]. ZnO is a wide bandgap semiconductor material extensively studied for its intrinsic properties but with limited industrial use as a UV-blocker in sunscreen creams and lotions, mixed varistors, solar cells, partially as laser sources, optoelectronics, in gas sensors, and also as catalysts for numerous types of organic reactions [26].

All the listed properties and applications of certain MONPs described in the previous sections are closely related to the structure, size, and shape of the nanostructures. It is clear that a large number of factors will influence the structural characteristics and main properties of the functional devices which will affect their performance. When combining two different nano-oxides including the development of *p*–*n* junction or modifying them with a dopant, elaboration of a nanostructure with optimal optical or electronic properties becomes a complex task. Moreover, the suitable method for fabrication MONPs with tunable structural parameters and properties should include optimization of all process parameters which could result in adverse alteration of the obtained characteristics. The existence of such a large number of factors influencing the structural characteristics and performance of the functional devices results in difficulties in reproducing the results obtained.

3 Nano-oxides in diverse applications

Presently, sensor technology is one of the important technologies and with continually growing applications, both in government and private sectors it could be on top as a future technology for the coming decades. More and more gas sensors are applied for environmental monitoring, semiconductor, health care, and automobiles. Therefore, the development of ultrafast and highly sensitive gas sensors with very small cross-sensitivity is the focus of the intense research, driven by strategies based on nanoscience and nanotechnology. Nanostructured materials especially nanoparticles with smaller dimensions have demonstrated a greater potential for use as key sensing layers.

3.1 Gas sensors

Developing highly performing, ever reliable gas sensors that can monitor accurately at or close to room temperature (RT) is becoming a priority in the gas sensor research. With some distinguishing advantages, such as larger range of operative parameters to be analysed (rapid fluctuations in light intensity, polarization, wavelength modulation, etc.), selectivity improvement, and easy implementation, MONPs allow better signal transport, in situ monitoring, and potential to be exploited by using surface plasmonic resonance which improves the sensing performance. Traditionally, over the past decades, metal oxide semiconductors (MOS) are the most commonly exploited sensing materials with advantages like a fast response, low cost, ease of handling, a wide range of target gases, and longer lifetimes. However, they also suffer from disadvantages like higher energy consumption and lower selectivities.

Owing more surface active sites, large surface-to-volume ratios, high specific surface areas with very high surface reactivity, and nano-metal oxides are applied towards gas sensing [27, 28]. Usually, a gas sensor that uses MONPs consists of a heating layer or wire (to obtain the optimum working temperature), conducting electrodes (that measure the resistance), and sensing film which changes its resistance upon exposure (Fig. 2). Conductometric gas sensors change their electrical conductivity upon exposure to the target gas. While the transducer function is dependent on the microstructure of the oxide, the receptor function depends on the gas–solid interactions and could be modified by mixing different oxides or adding noble metals. The gas sensing mechanism is defined by the number of reactive surface sites and adsorption of oxygen species that further increase the number of surface reactive sites [29]. The surface conductivity of the metal oxide is very much dependent on the surface stoichiometry because oxygen vacancies increase the surface conductivity, whereas absorbed ions decrease it. Upon adsorption of molecules such as O_2 or NO_2 at vacancy sites of the oxide, the electrons are flowed out from the conduction band and conductivity decreases, whereas CO or H_2 in the oxygen-containing atmosphere react with adsorbed O_2 releasing electrons and increasing conductance. The

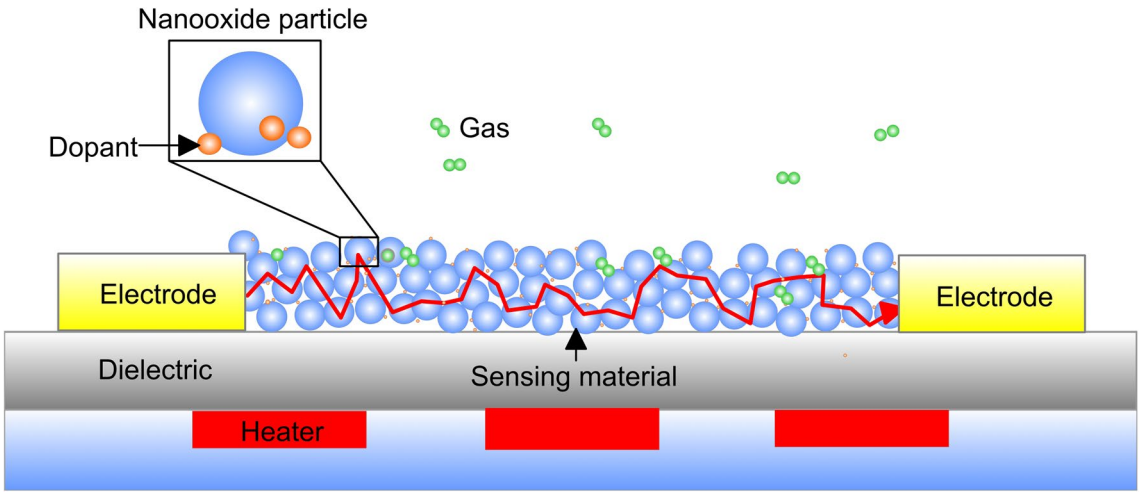

Fig. 2 Schematic representation of conductometric gas sensing device and sensing principle. The interaction with the surrounding atmosphere changes the conductivity of metal oxide and because of its transducer function electrical signal is transmitted to the electrode. The indirect heating of the device is used to change its electrical conductivity

adsorption reactions and abrupt temperature change of the sensor continuously alter the conductance. It follows that the optimum temperature is directly related to the reduction in metal and release of conduction electrons to the conduction band [30]. To have control of the rate-limiting reaction, heating of the gas sensor is used. The sensor response at low temperature is controlled by the speed of chemical reaction and at high temperature—by the speed of molecule diffusion [31]. In optimum temperature, the speed of both processes is equal while the response is setting maximum levels. In conductometric sensors, the heating could be direct or indirect but the latter is preferable due to higher stability and lack of interference with the sensing layer. However, working at higher temperatures not only increases the cost of power consumption and technical complexity of the device, but it could change the oxide properties leading to reduced stability and lifetime of the sensor.

The conductivity of a MO_x-based sensor depends on the particle size, their interconnected boundary characteristics (barriers, cross sections of the channels, etc.), the spatial organization of the nanoparticles (hierarchical, branched dendritic), *p–n* junction between the nanocomposites (heterostructures), etc. For nanocomposites, an increase in the conductivity response is usually found near the solubility limit of the second metal where a maximum structural disorder exists depending on the synthesis method and annealing [32]. Usually, the solubility limit of the most metal oxides varies between 1 and 5%. Increasing the surface area of the sensing film, the gas sensing performance increases which give rise to the production of relatively loose film structures or porous nanostructures such as nanotubes, nanospheres, nanowires, nanosheets, etc. [33]. Such hollow structures are usually produced by using anodizing processes, wet chemical methods, hydrothermal, or sol–gel synthesis. Some examples for such structures, their chemical composition, morphology, and sensitivity towards certain gases are summarized in Table 1.

Doping is another concept to change the electrical resistance and enhance the catalytic properties, because of produced smaller-sized doped metal oxides, catalytic activity, formed *p–n* heterojunctions [65] or obtained higher activity by increasing the density of the functional groups. Introducing the second component (noble or transitional metal, transitional or non-conductive nano-oxide or certain impurity) produces structural disorders of the metal oxide which lead to a significant reduction in the energy gap [32]. Gas sensing is receiving collective consideration in industrial production, biomedical applications, in hospitals and for environmental monitoring [66]. Good performance of a gas sensor is indicated by factors such as high sensitivity, rapid lower response time, low energy consumption, signal stability, long-term monitoring, and good reproducibility [67]. Typical examples of gas sensors for different gases based on semiconductor nano-oxides are discussed in the following sub-sections.

3.1.1 Carbon dioxide gas sensors

Carbon dioxide (CO_2) sensors are obligatory in countless fields, from monitoring air quality to hospital indoors and the food packaging industry. The parameters for these sensors in terms of performance, linearity range, the limit of detection and price vary significantly, depending on the field in which it is utilized. CO_2 sensors are widely required

Table 1 Gas sensing properties of metal oxides with different morphology

Target gas	Sensing metal oxide	Morphology	Sensitivity	Optimal temperature (°C)	References
H_2	SnO_2	Nanowiskers	10 ppm	300	[34]
	SnO_2	Nanorods	100 ppm	150	[35]
	SnO_2	Nanowires	10 ppm	300	[36]
	ZnO	Nanorods	500 ppm	25	[37]
	ZnO	Single nanowire	200 ppm	RT	[38]
H_2S	In_2O_3	Single nanowire	1 ppm	120	[39]
	In_2O_3	Nanowires	200 ppb	RT	[40]
	ZnO	Nanorods	50 ppb	RT	[41]
	ZnO	Dendrites	10 ppm	RT	[42]
	WO_3	Nanowires	1 ppm	250	[43]
NO_2	In_2O_3	Nanowires	1 ppm	250	[44]
	In_2O_3	Flowerlike coupled with rGO sheets	1 ppm	RT	[45]
	SnO_2	Nanowires	0.5 ppm	200	[46]
	ZnO	Nanowires	10 ppm	300	[47]
	Dopped ZnO/CuO with 1 wt% In_2O_3	Mesoporous	1 ppm	RT	[48]
	TeO_2	Nanowires	50 ppm	26	[49]
	CuO	Nanowires	2 ppm	300	[50]
	CdO	Nanowires	1 ppm	100	[51]
	V_2O_5	Nanofibres	1 ppb	300	[52]
	ZnO	Nanowalls coupled with rGO nanosheets	50 ppm	RT	[53]
NH_3	SnO_2	Single nanowire	100 ppb	300	[54]
	SnO_2	Nanorods coupled with rGO	200 ppm	RT	[55]
	WO_3	Nanowires	10 ppb	RT	[56]
	Au-modified ZnO	Nanosheets	10 ppb	260	[57]
	ZnO	Nanowire coupled with rGO	50 ppm	RT	[58]
CO	CuO	Nanowires	30 ppm	300	[59]
	CuO	CuO coupled by rGO hierarchical nanocomposite	1 ppm	RT	[60]
	SnO_2	Single nanowire	100 ppb	300	[61]
	ZnO	Nanowires fuctionalized with SnO_2	300 ppm	350	[62]
	Au-doped In_2O_3	Nanowires	200 ppb–5 ppm	RT	[63]
	$NiSb_2O_6$	Nanorods	300 ppm	300	[64]

for many offices indoors, industrial purposes, and environmental monitoring.

Because of their chemical stability, conventional metal and binary metal oxides display low sensitivity to inert gases such as CO_2. Different semiconductor nanomaterials have been tested for CO_2 detection and most of them indicated ineffectiveness in improving sensor response by doping. It is for this reason that researchers focused on new nanocomposite MO_x developed to meet this challenge. Combination of semiconducting oxides CuO–$Cu_xFe_{3-x}O$ nanocomposite (with $0 \le x \le 1$) was prepared by RF sputtering from a delafossite $CuFeO_2$ and used as a new active layer for CO_2 sensing. At different working temperatures (130–475 °C), the response of the sensor in a carbon dioxide atmosphere was measured by varying concentration up to 5000 ppm, and in different frequencies (0.5–250 kHz). The results obtained for a CO_2 concentration of 5000 ppm indicate a high response of 50% ($R_{air}R_{CO_2}^{-1} = 1.9$) (at 250 °C and 700 Hz) [68].

$BaTiO_3$–CuO-sputtered thin films were used for carbon dioxide sensing. The $BaTiO_3$–CuO sensor response towards CO_2 is due to a reversible reaction based on the presence of $BaCO_3$ in the composite material. Resistance and capacitance changes are closely associated with the work function changes in the *p*–*n* heterojunctions between $BaTiO_3$ and CuO [69]. Measuring impedance changes allows monitoring of the variations in CO_2 concentrations. The optimal working frequency range was

obtained from a frequency response via spatial charge and relaxation phenomena [70].

3.1.2 Carbon monoxide gas sensors

Carbon monoxide (CO) is a toxic, odourless, colourless, and tasteless (therefore, undetectable to human) gas slightly less dense than air. Encountering with ≥ 25 ppm concentrations, normal animal metabolism produces it in very low volumes and CO is thought to have some biological functions. Carbon monoxide is obtained from the partial oxidation of carbon-containing compounds, usually when there is not enough oxygen to completely oxidize and produce carbon dioxide (CO_2), as an indoor stove and internal combustion (IC) engine with a confined space.

CO gas sensor is an important primary instrument of detecting the toxic gas. To improve the sensitivity, stability, and response time and to reduce operating temperature, noble metals such as Pd, Au, and Ag are used as dopants in metal oxides gas sensors. For example, SnO_2 doped with Pd materials were realized in thick-film technology, stay while sensing CO. Sensing CO with SnO_2 sensors in the presence of humidity seems to be very ideal and aid in inferring the basic principles of metal oxide-based gas sensors [71]. However, this sensitivity to humidity makes it not applicable to variable humidity conditions whereas the high cost greatly limits the application of these noble metal-doped gas sensors. Pure SnO_2 and In_2O_3 were also used in detecting toxic CO gas at RT. Materials were produced using DC sputtering in an argon atmosphere (inert condition) by rheotaxial growth and thermal oxidation (RGTO) technique and with a reactive magnetron sputtering (RMS) in Ar and O_2 atmospheres, respectively. The sensor showed a linear response within the concentration range of 100–400 ppm of CO [72]. Pt/stabilized zirconia, YSZ/Pt, seems to be highly sensitive to a limited amount of CO in an O_2-containing gas stream. The electrochemical measurements carried out by means of steady-state polarization curves in the temperature range of 500–650 °C indicated good CO sensing characteristics in the concentration range of 32–800 ppm of CO in the air [73]. Ag–ZnO/MoS_2 ternary nanocomposite CO sensors were fabricated by layer-by-layer self-assembly route and compared with pure ZnO, ZnO/MoS_2, and Pt-ZnO/MoS_2. Ag–ZnO/MoS_2 nanocomposite film showed the highest response among four tested sensors towards CO gas at RT which fact was attributed to the catalytic activity of Ag and synergistic effect of ZnO and MoS_2. This nanocomposite sensor had shown an excellent response time, swift response/recovery characteristics, good selectivity, and repeatability [74].

TiO_2-reduced graphene oxide (rGO) nanocomposites synthesized in situ via hydrothermal route using graphene oxide (GO), $TiCl_3$, and NH_3 solution were also used for CO sensing. The TiO_2-rGO nanocomposites showed a linear response for sensing CO gas in the range 100 and 200 ppm [75]. Other authors investigated the sensing properties of copper oxide (CuO)/graphene hierarchical hybrid nanocomposite towards CO gas. The sub-ppm-level CO gas sensor was fabricated by layer-by-layer self-assembly route. The sensor exhibited a high response, good reversibility, fast recovery times, and repeatability for carbon monoxide gas sensing. At RT, CuO/graphene nanocomposite exhibited not only excellent detection abilities but also good stability and selectivity over a wide range (from 0.25 to 1000 ppm) concentration of CO [76]. It seems that the performance of hybrid graphene–nano-oxide nanocomposites indicates the best performance with higher responses to CO at low concentrations and low temperatures.

3.1.3 Oxygen gas sensors

As life-sustaining gas, oxygen sensors are used in numerous fields, for instance, hospitals, in industrial measurements, manufacturing installations, foundries, monitoring, and control of large-sized combustion furnaces. Recent improvements in the development of O_2 sensors increased mainly for automotive industries and hospitals. Three existing variants of O_2 sensors: say, semiconductor oxides (TiO_2 sensors), concentration cell (Zr-based sensors), and electrochemical pumping O_2 sensors (based on limiting current), are presently available to control the engines air–fuel ratio. For the purpose of controlling and sensing O_2, semiconductor oxide sensors (TiO_2 sensors) and solid-state sensors (Zr-sensors) are chosen due to a smaller size, less expensive, outstanding reliability, and high stability.

Oxide materials such as TiO_2, CeO_2, and Nb_2O_5 semiconductors have been used as O_2 sensors based on the difference in resistance caused by reduction or oxidation of the semiconductor depending on the oxygen partial pressure in the circumvent ambient atmosphere [77]. TiO_2 sensor indicated a delay as opposed to that of a ZrO_2 sensor for its limited durability and poor accuracy. However, when compared to ZrO_2 sensors, TiO_2 sensor showed superior tolerance towards oxygen. For that reason, the growth of TiO_2-based sensors improved and a few industrial units had adopted these [78]. Sputtered Nb_2O_5 thin films deposited on an Al_2O_3 substrate, expended some advantages like swift signal reception and very precise operation close to RT or low temperatures, whereas thin-film Nb_2O_5 sensor's response time at ambient conditions in comparison with a ceramic TiO_2 sensor (unheated) and a conventional ZrO_2 sensor (unheated) was inferior [79]. Few more appropriate metal oxides such as CoO [80], Co_{1-x}, Mg_xO [81], and $SrMg_xTi_{1-x}O_3$ [82] semiconductors were used in monitoring oxygen.

3.1.4 Ozone gas sensors

Ozone (O_3) is an oxidizing agent having significant countless real-world usages. Primarily, O_3 measurements are required for medical applications, pharmaceutical, biotechnological and chemical processes, food product handling and packing, in research laboratories, water decontamination, etc. However, as a powerful oxidizing reagent, ozone appearance in the ambient atmosphere is very dangerous to the health of humans. It could cause eye irritations, headaches, respiratory problems, and even damage to the lungs. The continuous exposure to 0.1 ppm O_3 for 2 h caused a decrease in spirometry (a loss of 20% in breathing capacity) lung function [83]. It follows that the extensive use of O_3 creates a strong demand for a simple but highly sensitive method for monitoring the ozone concentration in the atmosphere under many conditions.

A number of approaches for monitoring O_3 concentrations that include electrochemical [84], optical [85], resistance method [86], but also other technologies like impedance spectroscopy [87] and photoreduction under UV light [88] were proposed. When introducing ozone to n-type oxide, it fills the vacancies and reduces the MO_x which decreases its conductivity. To synthesize cheaper than noble metal-doped sensors, people are trying to explore composite-based semiconductors gas sensors that benefit the sensitivity and response time at room temperature. For the detection of ozone in the air, TiO_2–SnO_2 sensing materials in different ratios were examined. Working at RT, the 1:4 mixture of TiO_2–SnO_2 had shown the highest sensor response units of 327. When adding noble metals such as Au (0.5 wt%) to TiO_2–SnO_2 (1:4) to detect O_3 by photoreduction method and to enhance the signal, the ozone response was boosted to 6.6×10^6 (nearly $10^4\times$), whereas the response signal and recovery times were lessened by 35 and 5 s, respectively [89]. The same research group has studied the carbon nanotubes (SWCNT) incorporation with In_2O_3 materials for rapid trace detection of ozone with concentration from 25 ppb to 2.5 ppm at RT. The highest sensor response of 13.21 for 1500 ppb O_3 was obtained for 2.0 wt% SWCNT-In_2O_3. The produced SWCNT-In_2O_3 exhibited reproducibility, stability, excellent reversibility, and selectivity for O_3 at RT, which made it one of the best sensing material with promising application in the field of ozone detection [90]. Composite materials containing different weight ratios of TiO_2–WO_3 and Au-doped TiO_2–WO_3 was used for the detection of O_3 gas while employing a light source of blue LED (460 nm). The 3:1 TiO_2–WO_3 weight ratio exhibited the highest sensor response that was promoted to 23.8 towards 2.5 ppm O_3. Adding Au (0.1 wt%) to 3:1 ratio of TiO_2–WO_3 elevated the response of the sensor to 64. The sensing properties of O_3 were attributed to the mechanism of photoreduction, adsorption and desorption, and surface reactions of O_3 [91].

ZnO nanorods grown by CVD method was also subjected to O_3 sensing. Among several ZnO nanomaterials, the former displayed interesting and promising results with a fast response time of 1300 and short recovery times of $T_r = 60$ s and $T_{rec} = 5$ s, respectively, measured for a concentration of O_3 varying from 1 to 2.5 ppm [92]. Photostimulated nano-In_2O_3-based compact and energy-saving ozone sensors were capable of detecting O_3 with a wide dynamical range over four orders of magnitude at RT. By examining the rate of change of resistance, it was found out that the responses to fixed O_3 gas concentrations for 5 min, 1 min, and 30 s were uniform and linear in proportion to O_3 gas concentration. This linearity continued in a concentration range from 10 ppb to 200 ppm. The cross-sensitivity to CO, CO_2, and NO_2 of the photostimulated O_3 sensor was very low. In addition, the sensing signal was highly reproducible without indicating hysteresis effects during repeated measurements [93].

3.1.5 Methane gas sensors

One of the important natural gas components is methane (CH_4), readily found in the environment. Because of its lower explosion limit of 5.0%, methane is used in diverse day-to-day applications [94]. Metal oxides are proved to be potential functional nanomaterials with application in cheap chemical gas sensors. Sensing methane with highly ordered mesoporous In_2O_3 that replicates the structure of cubic KIT-6 SiO_2 and hexagonal mesoporous SBA-15 SiO_2 was investigated. Not only the pore sizes and thicknesses of pore walls in the mesoporous materials but also the nanoscopic properties of the sensors correlated to the methane sensitivity. The highest sensitivity to CH_4 gas was shown to be in concentrations pertinent for prevention of an explosion. As the high thermal stability is vital for a gas sensor, In_2O_3 materials turned out to be highly stable methane sensing materials between temperatures of 450 °C and 650 °C [95].

Modifications with Pt or Pd are applied widely for methane monitoring as they exhibit catalytic activity lowering the activation energy for the reaction with gas. For example, in contrast to pristine SnO_2, Pd doped SnO_2 with 1.5 mol% Pd showed a higher response (75 and 95%) towards LPG at an operating temperature of 50 and 100 °C, respectively. The authors attributed this effect to Pd-enhanced formation of nanospheres at a calcination temperature of 500 °C, a decrease in crystalline size down to 11 nm and the catalytic effect of Pd [96]. Researchers also synthesized a hybrid composite of nanocrystalline zinc oxide (ZnO) and reduced graphene oxide (rGO) by a facile hydrothermal process for sensing methane gas. At

an optimal operating temperature of 190 °C, the ZnO–rGO film sensor coated on a ceramic tube with Ni–Cr heater indicated detection of methane from 100 to 4000 ppm together with excellent repeatability, fast response-recovery time and good selectivity [97].

3.1.6 Nitric oxide gas sensors

Nitrogen monoxide (NO) is highly reactive gas that participates in many complex chemical and biochemical reactions. It is a vital messenger molecule, which has been the molecule of interest during the past decades. NO is both beneficial and detrimental. Due to its high reactivity, it is an enormously significant intermediate of the in-process chemical industry and an essential signal molecule, triggering grave toxicity in the mammals' body.

In nitrous oxide sensing, WO_3 is the most widely used oxide material because of its largest response. For improving the performance of WO_3-based sensors, various nanocomposites with promising performance have been constructed. For instance, 4:1 (by weight) optimized In_2O_3–WO_3 nanomaterials prepared by sol–gel and calcination methods were used to monitor NO gas at RT (300 K) on gas sensor chips prepared by the screen-printing method. The thin film of nano-In_2O_3–WO_3 composite coated two comb-like inter-digitated gold electrodes with thoroughly platinized edges. We found that this NO gas sensor showed response and recovery times less than 30 and 40 s, respectively, together with very good linearity even in 100–1000 ppb concentration range. The nanocomposite In_2O_3–WO_3 sensor was able to detect ppb to sub-ppb ultratrace levels of NO at RT. It showed sensor response equal to $S = 9205$, good reversibility (less than 3 s) without shift when purged with nitrogen gas, and extremely high selectivity for a known concentration of 500 ppb NO [98]. In another study, different In_2O_3–WO_3 nanocomposites were synthesized and optimized to a 4:1 ratio which was much better than other compositions towards sensing NO. The metal oxide (4:1) composite and 0.25% Pt-doped In_2O_3–WO_3 (4:1) coated over screen printed gold electrodes acted as RT sensors. Our results showed that the sensor response ($S = R_{NO}\, R_{N2}^{-1}$) at RT towards 1000 ppm of NO was 23.9 while the response and recovery time were 12.5 and 15.3 min, respectively. Advancing this with an extra 0.25% Pt loading, the response of the sensor was boosted; for 0.1 ppm and 25 ppb, it was 330 and 15.2, respectively. The NO sensor optimal linear range was in the concentration range of 25–100 ppb [99]. It follows that the noble metal doping together with optimizing new nanostructured composite ratio and device design offers new possibilities and address the challenge of significant improvement in sensor performance. The capability of accurate NO sensing in the ppb range provides certainty within the save limit for the human.

3.1.7 Nitrogen dioxide gas sensors

Rapid industrialization, urbanization irregular growth of population, uncontrolled anthropogenic activity, escaping toxic volatile chemicals and gases, from vehicular fuel combustion, excessive use of insecticides, and pesticides in the agricultural sector caused the rise in gaseous pollution levels. This is becoming an alarming threat to the ecological systems present in the biosphere. Nitrogen dioxide (NO_2), a reddish-brown pungent oxidizing gas, enters the atmosphere either through natural sources or anthropogenic activities. The second one contributes substantially to reasonably high loads of NO_2 gas into our atmosphere. The increasing consumption of fossil fuels in automobiles and industries sends into the atmosphere a large number of NO_x. NO_2 is considered as a secondary pollutant generated from primary NO source that is produced as a result of internal combustion engines.

Various metal oxide nanoparticles such as SnO_2, WO_3, TiO_2, ZnO, etc., have been subject to NO_2 gas sensing. For example, SnO_2 nanoparticles synthesized from ethyl hexanoate precursor were directly used as a thick-film NO_2 gas sensing. They were extremely crystalline with a low degree of aggregation and 17 nm crystallite size. The drop coating deposited particles indicated a fast and stable response at NO_2 concentration below 200 ppb. The flame-pyrolysed SnO_2 nanoparticles exhibited high sensitivity and rapid response to both propanal (reducing) and NO_2 (oxidizing) gases [100]. Using sol–gel spin coating process, Indium (In)-doped SnO_2 thin films with a particle size of about 3 nm and different doping concentrations were deposited on float glass substrates. The selectivity and response of NO_2 gas sensor at low operating temperature were improved with In-doping that triggered also a decrease in agglomeration which process could cause lower stability and an increase in response time of the small-sized particles. 10 wt% In-doped SnO_2 films demonstrated an extremely high sensor response (~ 7200%) towards 500 ppm of NO_2 gas at 150 °C [101].

When evaporating W filament under a low pressure of O_2 gas, monoclinic WO_3 nanoparticles were obtained. Their size proportionally increased with oxygen pressure and annealing temperature. Comparatively, the decrease in the size of WO_3 particles caused an increase in NO_2 sensitivity. 36 nm sized WO_3 particles displayed the highest sensitivity, 4700 to 1 ppm NO_2 gas, at a temperature moderately above RT-50 °C [102]. In another study, reactive gas deposited WO_3 porous nanocrystalline films, both pure and activated (doped) were subjected to NO_2 gas sensing. Activation was done by co-evaporation of Au

or Al with WO_3, nanoparticles. With the increase in sintering temperature from 100 to 600 °C, the tetragonal phase changed to monoclinic. As regards to activation, doping with Al was found to be more effective at RT whereas Au was suitable for higher temperatures. The selectivity of the sensors for NO_2 was around ppm level with optimum sensing temperature of around 252 °C [103].

Recent studies revealing the gas sensing properties to NO_2 of ZnO nanoparticles identify them as promising sensing materials. For example, ZnO nanoparticles with sizes ranging from 5 up to 270 nm were obtained by annealing at four temperatures (200–800 °C, with an increase of 200 °C) a zinc carbonate hydroxide (CH_4O_5Zn) precursor. The ZnO annealed at 400 °C exhibited the highest selectivity to NO_2, good optical properties, quick response time towards NO_2 sensing (≤ 30 s) and good recovery (≤ 120 s) [104]. Hydrothermally synthesized ZnO NPs from $Zn(OH)_2$ also showed a good response at RT for NO_2 gas of concentration of 5 ppm. In contrast to other tested gases such as CO and ethanol, the response towards NO_2 did not increase with the increase in temperature [105]. In another study, neck-based ZnO semiconductor NPs were used for sensing NO_2 gas. The necked-ZnO NP sensors response was 100 when subjected to 0.22 ppm of the oxide at a temperature of 200 °C and increased to about 400 when the concentration of NO_2 increased to 5 ppm. T_{90} and Tr_{90} times for NO_2 gas sensor were found to be 13 and 10 s, respectively. Stable response features of the sensor were displayed under repeated studies with NO_2 gas with a concentration of 0.4 ppm [106]. Sol–gel-synthesized ZnO films exhibited very high selectivity, sensitivity, and rapid response towards NO_2 gas at an operating temperature of 200 °C, but the response towards concentration from 10 to 100 ppm of NO_2 varied. The high operating temperature led to high adsorption density of O- and O_2 and, therefore, fast gas response (maximum of 75% at 200 °C) and recovery times [107].

Pristine TiO_2 anatase nanoparticles and N-doped TiO_2 anatase nanoparticles were used to tap and compare the potential of N-doped nanoparticles for sensing and removal of NO_2 molecules. The possible orientations of NO_2 molecules towards N-doped TiO_2 and Van der Waals (VdW) interactions were taken into account to reveal the most geometrically stable NO_2–TiO_2 complexes. The structural and electronic analysis found out that N-doped particles provided a more stable configuration of the analysed complexes and consequently formed efficient absorption complexes suggesting greater sensitivity [108].

3.1.8 Ammonia gas sensors

With a distinctive pungent odour, ammonia (NH_3) is a colourless gas which represents the simplest pnictogen hydride. Very common in nitrogenous waste, mostly among aquatic organisms, it contributes meaningfully for the nourishing demands of surface-dwelling living beings as a precursor to food and chemical fertilizers. For that reason, different MONPs such as ZnO, SnO_2, and In_2O_3 have been examined as NH_3 gas sensors. Among them, SnO_2 immerged as promising ammonia sensors. For example, cluster matrix of SnO_2 NP consisting of thousands of extremely small-sized (~ 3.0 nm) SnO_2 NPs and randomly distributed wormhole-like pores interconnecting the oxide NPs was used for sensing ammonia. As previously mentioned, incorporating of noble metal catalyst could improve the sensing properties. Hence, Pt-activated SnO_2 NP clusters incorporating the element in two forms—metallic (Pt) and metal oxide (PtO_2), were synthesized. Unlike the as-synthesized pure SnO_2 nanoparticles by a solvothermal method, Pt-activated clusters demonstrated enhanced gas response from 6.5 to 203.5 towards 500 ppm of NH_3. The authors concluded that Pt-doped SnO_2 possessed good response–recovery times, selectivity, linear dependency rates, repeatability, extremely high sensitivity, and long-term stability, ascertaining the prospective application of the examined clusters for NH_3 sensing [109]. In another study, molybdenum disulphide (MoS_2)/tricobalt tetraoxide (Co_3O_4) nanocomposite film-based sensor was fabricated towards NH_3 detection. The MoS_2/Co_3O_4 film sensor enhanced the ammonia sensing properties at RT in ultralow concentrations as opposed to MoS_2 and Co_3O_4 counterparts because of its layered structure, *n*–*p* heterojunction formed and synergistic effect of the compounds [110]. The same authors were even able to synthesize a film sensor by hydrothermal and layer-by-layer self-assembly method recognizing and predicting both components in a mixture of two gases—ammonia and formaldehyde. A neural network-based model was used for investigating the sensing properties of MO_x/graphene composite towards the mixture of gases such as dynamic response, sensitivity, stability, and recovery time at RT [111].

3.1.9 Hydrogen sulphide gas sensors

Hydrogen sulphide (H_2S) is toxic flammable, colourless, explosive, naturally occurring in petroleum rigs, natural and volcanic eruptions, and hot-bath springs. If heated under pressure, it will explode. In contact with the organism, the gas causes inflammation and irritation to eyes and respiratory system. Any process that breaks down organic material without oxygen, produces heavy water or processes food and petroleum, has the potential to create high levels of H_2S. Here we have considered the basic limitations of sensor types for quantifying H_2S in terms of major operational

criteria (e.g. the limit of detection, response time, the common operating range of concentrations, and stability).

Accurate measurement of H_2S in real time at low micromolar or nanomolar concentrations has been a long-term challenge. In 2005, researchers from the University of Alabama at Birmingham have developed a novel polarographic H_2S sensor that detects rapid changes in the concentration of H_2S in biological solutions having a detection limit of 10 nm. [112]. H_2S sensor is a metal oxide semiconductor that changes the resistance that is normally produced by desorption and adsorption of H_2S in a film. This thin film can be a gold thin film or tin oxide film that is sensitive to hydrogen sulphide. The current response time of H_2S sensor ranged from 25 ppb to 10 ppm, which was less than 1 min. Commonly, an ultrahigh sensitive hydrogen sulphide sensor is used currently which employs micromachined nanocrystalline SnO_2–Ag. SnO_2–Ag nanocomposite was fabricated by a polymeric sol–gel process so that the sensor exhibited outstanding sensing features upon exposure to H_2S of just 1 ppm at temperatures of 70 °C (158 °F) while being very less sensitive to gases like C_6H_{14}, SO_2, HCl, etc. The better sensitivity, as opposed to pristine SnO_2, was attributed to the dissemination of AgO at the grain boundaries of SnO_2 nanocrystals and the achieved *p*–*n* junction. The environmental influence on sensors sensitivity and selectivity indicated a small risk of false alarm [113]. Not only noble dopants but also transitional metals have been also used as an activator for SnO_2 NPs subjected to H_2S sensing. Vaishampayan et al. (2008) compared H_2S sensing performance of 40 nm sized pristine SnO_2 and 18 nm sized Fe-doped (1 at%) SnO_2 synthesized by a simple modified pechini citrate route. In contrast to the negligible response towards H_2S of SnO_2, Fe-doped SnO_2 was capable to detect even 10 ppm of H_2S at RT. Since the high surface-to-volume ratio of NPs, the doped sensor exhibited fast response within 5–15 s with a change of about one order of magnitude in the resistance [114].

The sensitivity of semiconducting SnO_2-based gas sensors has been investigated by engineering of the base material and with the incorporation of CuO as an additive. By optimizing the grain size and the amount of CuO loading the sensor elements were sensitive to concentrations of $H_2S \sim 10$ ppm in the air while the operating temperature was reduced down to about 90–100 °C which lowered the energy consumption [115]. It was found that hydrothermally synthesized *n*-type SnO_2 nanorods coated with *p*-type CuO NPs were particularly sensitive at lower temperatures (60 °C), with the highest sensitivity (9.4×10^6) to 10 ppm H_2S [116]. The sensing towards H_2S via semiconducting CuO nanoparticles included conversion to metallic CuS, following the reaction:

$$CuO + H_2S \rightarrow CuS + H_2O.$$

For *n*-SnO_2/*p*-CuO heterojunction H_2S gas sensor, the exposure to hydrogen sulphide gas led to a chemical transformation of *p*-CuO into highly conducting Cu_2S declining noticeably the barrier height and changing immediately the resistance [117]. The suitability of the proposed modification was further confirmed by the highly selective and sensitive ($\sim 10^6$ to a few ppm levels) responses of CuO-doped thin film of SnO_2 obtained by a thermal evaporation method to H_2S in the air. The long-term stability for a period of over 3 years time in response to H_2S gas was further assessed at four different operating temperatures [118].

The effectiveness of doping different MONPs with noble metals for enhanced H_2S sensing performance was confirmed by other studies. WO_3 doped with platinum (Pt), gold (Au) or Au–Pt noble metals were used for H_2S sensing. At operating temperature of 220 °C and 1 ppm H_2S gas concentration, individual sensitivities of 23 and 5.5 were measured for Pt- and Au–Pt-doped WO_3 gas sensors, respectively. Pt- , Au- , and Au–Pt-doped WO_3 thin films indicated sensor response times of 30, 8, and 2 s, respectively, whereas the recovery times were about 30, 160, and 30 s, respectively [119]. Doping 0.5 wt% Pd with 5 wt% Al_2O_3 and mixing with anatase TiO_2, outstanding sensitivity was observed for low concentrations of H_2S. H_2S sensor using TiO_2/Al_2O_3/Pd as sensing materials demonstrated high sensitivity and undesirable cross-sensitivity effects when checked for NO_2, LPG, CO, CO_2 and H_2 gases detection [120].

Performance of α-Fe_2O_3 NPs produced by post-thermal annealing of a facile Fe_3O_4 precursor as H_2S gas sensing material was examined at different operation temperatures (100–400 °C). At 300 °C, the sensor exhibited the highest sensitivity, reproducibility, and good stability while the limit of detection was measured to be 0.05 ppm with response and recovery time of 30 s and 5 s, respectively [121]. Together with pure iron oxides, various transitional metal ferrites such as $CuFe_2O_4$, $CoFe_2O_4$, $ZnFe_2O_4$, and $NiFe_2O_4$ prepared by the citrate process have potential application as gas sensing materials not only for H_2S but also for CO, CH_4, Cl_2, LPG, etc. [122]. Sol–gel auto-combustion technique was used to prepare spinal ferrite $CuFe_2O_4$ NPs that were equally sensitive to both H_2S and H_2, but at low temperatures, they were highly sensitive to H_2S detecting concentrations of 25 ppm at 80 °C. In contrast to annealed at 500 and 750 °C nanoparticles with an average size of 36 nm, the 25 nm sized as-prepared NPs were the most suitable for H_2S sensing [123].

Recently, except semiconducting (pure, doped, or decorated) MONPs, for monitoring gases in the environment nanocomposites of metal oxides nanoparticles and carbon nanotubes have been tested. For sensing of H_2S gas species Co_3O_4 NPs and Co_3O_4 single-walled

carbon nanotube (SWCNT), nanocomposite structures were explored. Different wt% of Co nanoparticles were introduced into graphite tube to synthesize Co-SWCNTs that were further oxidized at different temperatures. The Co_3O_4-SWCNT composite structure produced by a co-arc-discharge method displayed improved performance in H_2S sensing than the pure Co_3O_4 nanoparticle structure due to the high defect density in the Co_3O_4 nanoparticles [124]. The large surface-to-volume ratio, small size, flexibility, and mechanical stability make these MO_x-carbon nanotube 3D heterostructures very attractive in ultrahigh sensitive sensors application. However, finding suitable and stable nano-metal dopant with reasonable high integration density and binding energy without affecting the transport and electronic properties of both materials is a challenging task.

3.1.10 Hydrogen gas sensors

The requirement of resources for clean energy towards fuel cells and IC engines can be drawn from hydrogen (H_2). Hydrogen energy shall form the infrastructure that will power future societies since it is a clean, cost-effective, and renewable source of energy. Nevertheless, hydrogen, being flammable gas, it has a lower explosion limit of 4% in air meaning that even a small spark can ignite the mixture. Therefore, hydrogen generation, transport and storage can be dangerous if not handled with caution, requiring high precision sensitive gas sensors which are able to detect the smallest leaks fastly. Semiconductor metal oxide gas sensors are an important candidate for the task of a sensor forming an acoustic early warning system, notifying the authorities or provide the signal to a process control system. To accomplish this, an accurate and stable in situ real-time measurement gas sensor is required. Nevertheless, using hydrogen as a fuel source needs innovative ways to store and monitor hydrogen. Reliable, precise hydrogen sensors that are compact and cheap are called for both quantifying the hydrogen concentration in continuously mobile gas streams and also for checking hydrogen gas leaks in ambient air. It is very crucial for the alarm sensors to detect hydrogen below the explosion limits.

A review by Gu et al. [125] gave a complete overview of the hydrogen sensing properties of metal oxides nanostructures, including thin films and 1D nanostructures. The majority of MO_x-based gas sensors suffer (a) low sensitivity and (b) lack of selectivity. To solve these, numerous strategies have been applied, such as the sensor's dynamic response analysis and mixed oxides sensors for gas detection [126]. The addition of noble metals like gold (Au), platinum (Pt) or palladium (Pd), to a semiconducting oxide, which is an effective means to boost detection of specific gases using metal catalysts shall increase the rate of interaction differently for distinct gases [127]. Platinum (Pt) is one of the most effective catalysts for sensing reducing gases, including hydrogen, carbon monoxide, and hydrocarbon, by chemical sensitization or spillover effect [128]. Together with it, several MO_x materials like, WO_3 [129], ZnO [130], TiO_2 [131], MoO_3 [132], and Nb_2O_5 [133] have been used. The newly designed and produced prototype sensor using ZnO–SnO_2 composite material was investigated for its gas sensing behaviour at dissimilar concentrations of hydrogen gas at various temperatures. The sensor cross-sensitivities from interfering gases like CH_4 and CO were also studied. It displayed very high selectivity, exceptional response times, and very good reproducibility towards hydrogen at 150 °C [134]. A ternary hybrid of palladium-tin oxide-molybdenum disulphide (Pd–SnO_2/MoS_2) was fabricated towards H_2 gas sensing. It indicated excellent sensing properties towards hydrogen at RT in the range 30–5000 ppm explained by the modulation of the potential barrier for electron transfer as well as the synergistic effect of hybrid nanostructure [135]. It could be concluded that in the mixed metal oxides, the combination of two-phase properties and oxygen vacancies contributes to chemical activation not only to H_2 but also towards NO, CO_2, CH_4, H_2S, etc.

Out of the studies reviewed, it follows that the elaboration of composite solid-state gas sensors should take into account not only the oxide nanocomposite ratio but also the chemical nature, distribution, size and specific concentration of the additives (modifiers) as well as nano-oxide–matrix pair because semiconductor oxides could change the configuration of *d*-electrons at the surface when transitional element have been used [136]. However, the optimum concentration on the additive and second component content in the nanocomposite may change depending on the operating temperature and/or humidity. It is, therefore, important to consider the thermodynamic stability of the system in different atmospheres triggering adverse temporal effects. Additionally, in many cases, the improvement in sensing parameters is closely related not only to the composition and operating temperature but also to the nano-oxides morphology and, therefore, optimized technological parameters when developing sensors. It follows that reproducible fabrication processes with precise control over the morphology and composition of the nano-oxides are strongly recommended.

3.2 Batteries

Rechargeable batteries gained noteworthy attention in the past years due to severe environmental concerns. Lithium-ion batteries (LIBs) play a major role in our life by excessively using in the field of portable electric devices, electric vehicles, and hybrid vehicles due to their very

high energy density and long life cycles. To enhance the performance of LIBs, researchers gave excessive prominence to develop novel electrode materials with nano-MO_x that have been used traditionally for several decades by researchers. Countless TMOs were expansively considered in LIBs as electrode materials. In terms of the reaction mechanisms, TMOs operate on two main principles (a) intercalation/deintercalation and (b) conversion reaction. In batteries, nano-TMOs are appealing anode materials because of their higher theoretical capacities than commercial graphite (372 mA h g^{-1}) [137]. TMOs are able to conduct conversion reactions and even complete phase transformations during charge–discharge cycles. Usually, the size of nanoparticles of conversion materials has a decisive influence on electrochemical properties, since smaller-sized oxides increase the capacity and rate of capability and reversibility. However, some nano-oxide anodes have poor cycling performance or electrical conductivity that could be enhanced by mixing them with electrolytes [138], combining them to form composites [139] or adding a thin layer of conducting polymer [140]. Presently, hierarchically nanostructured TMOs have turned out to be a thrust area of research in the field of LIBs, in which hierarchical architecture provides several available electroactive sites for redox reactions, accommodates the strains due to severe changes in volume throughout cycling, and shortens Li-ion's diffusion pathway during the process [141]. For instance, because of excellent redox properties and high theoretical capacity, cobalt oxides have drawn tremendous attention as electrode materials in batteries. When used as anode materials in LIBs, superior cycling reversibility and high discharge capacity were demonstrated by Co_3O_4 nanotubes synthesized on porous-alumina template technique [142].

TMOs are one of the first developed, oldest and quite significant materials for electrodes in SIBs. Many researchers focus their attention towards them for nearly three decades, particularly in the last 5–10-year period [143]. Rechargeable batteries have attracted major attention in recent years because of aggravating environment problems. LIBs play a vital role in our daily life and exclusively used from portable electronic devices to hybrid electric vehicles. Uneven distribution, limitation of lithium resources and their high-cost storage, however, gradually aroused people's anxiety on LIB sustainability. SIBs have been thought to be next-generation large-scale rechargeable batteries due to the earth abundance, relatively high safety and cost-effectiveness of sodium resources. The vital factor for commercializing the promising SIB rechargeables consists in the development of advanced and cost-effective anode materials. Because of the stable redox potential, high energy density and safety, metal oxides were found to be promising electrode materials for SIB [144].

However, some MO_x suffers from large volumetric expansion during electrochemical cycling of SIBs, low conductivity and cycling stability, and unsatisfactory capacity rate. Incorporation of graphene to MOs with the tailored nanostructure, crystal phase, and composition has demonstrated long cycling life, high energy density, and other promising performances as electrodes in SIBs [143]. In a composite, the MO_x provides high capacity and activity whereas graphene delivers easy processing and chemical functionality via electron conductive network suppressing agglomeration of the oxide and increasing the available surface for the electrochemical processes. Many MO_x/G composites offer unanticipated capacity synergy that helps to escalate storage capacity. For applications in LIBs, nanosized MO_x along with graphene are debated more beneficial integrated structure for shortening lithium diffusion pathways and plummeting polarization within the electrode, leading to boosted performance [145].

Recently, researchers focus on the synthesis of multiple (four or five) transitional cationic oxides in equiatomic amounts stabilized in single rock-salt structure or the so-called high entropy oxides (HEOs). They seem to be very promising materials in reversible electrochemical energy storage. In HEOs, only cation sublattice is altered while the oxygen sublattice stays unchanged (Fig. 3). In contrast to the first neighbours, the second near neighbouring atoms in the crystal lattice is different and unusual cation coordination values are present. The random distribution of cations in the solid solution gives stability towards phase separation. The probability of finding a cation on a given lattice site is equal to the atom fraction of the element [146]. Uncertainty in atoms positions could result in an unpredictable and nonlinear synergetic response that comes from an unusual combination of elements and microstructures. This will influence the distribution of lattice site energies, lattice distortions, sluggish diffusion, and the number of equivalent microstates [147]. The random distribution of cation species in their sublattice substantially increases the configurational entropy by composition. HEOs of (Cu, Co, Mg, Ni, Zn) O system are found to have very high dielectric constant [148], whereas the conductivity of Li-doped (Cu, Co, Mg, Ni, Zn) O is found to be orders of magnitude higher than that of the conventional solid electrolyte (LiPON) [149]. Using spray pyrolysis techniques (flame and nebulized spray pyrolysis) and wet chemical technique single phase (Co, Mg, Ni, Zn) O and (Co, Cu, Mg, Ni, Zn) O were directly synthesized in a nanocrystalline form [150]. The reversibility of the phase transformations between a polyphase mixture and homogeneous solid solution of different binary oxides that is proof for the

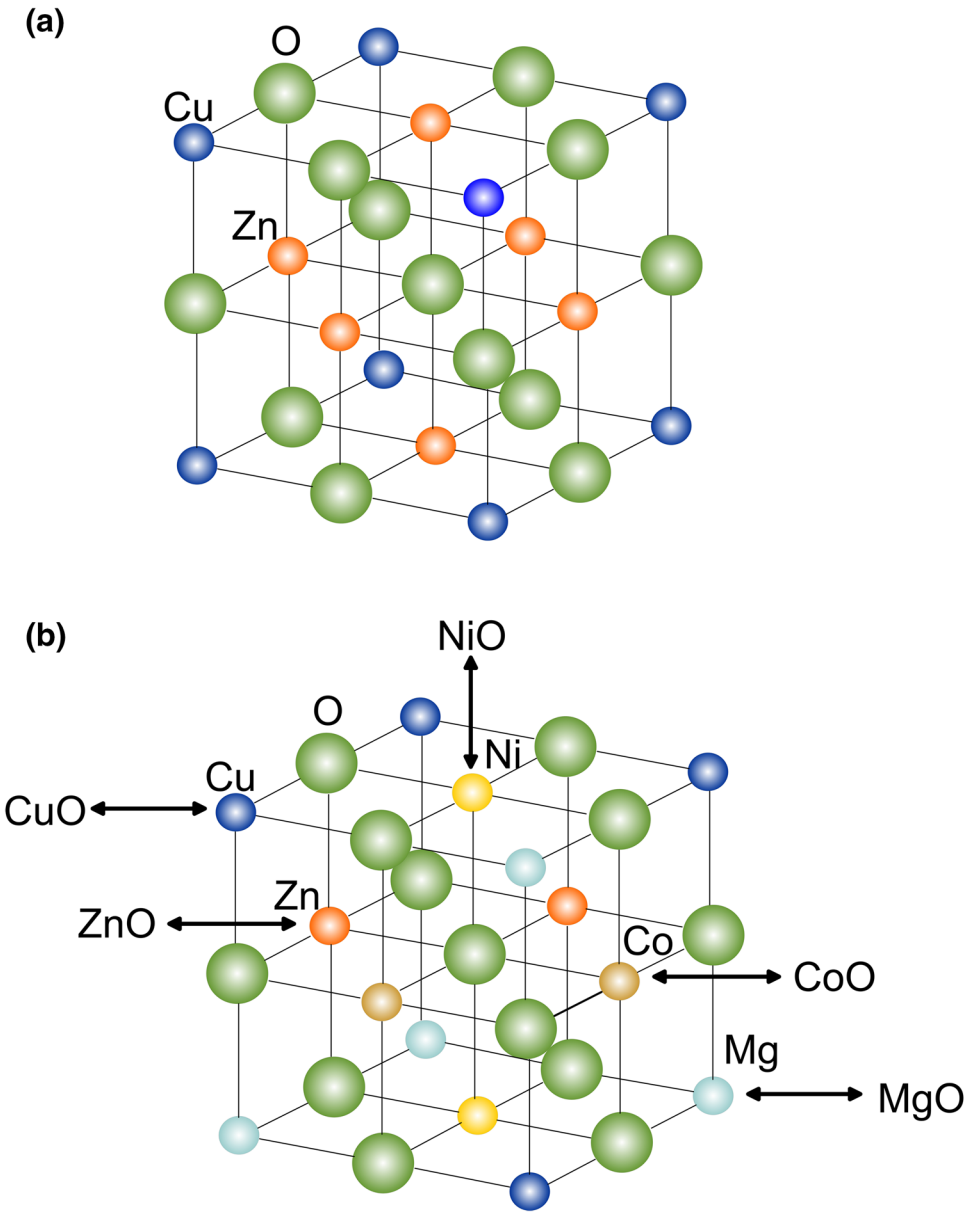

Fig. 3 Schematic of disordered arrangements of **a** random pseudo-binary Cu, Zn mixed oxide; **b** Cu, Mg atoms on the Cu sublattice and of Zn, Ni, Co atoms on the Zn sublattice of random pseudo-quinary mixed oxide. The random distribution of cations contributes to excess configurational entropy

effect of entropy on phase stabilization was confirmed by structural analysis. $(Co_{0.2}Cu_{0.2}Mg_{0.2}Ni_{0.2}Zn_{0.2})O$ was tested in secondary Li-based cells for complete or partial reduction in metal ions upon lithiation [151]. The cell reached a good capacity of 600 mA h g^{-1} subsequently increased to 650 mA h g^{-1} after 70 cycles. The exclusion of one of the elements from the five cation system and turning it to four cation system $(Cu_{0.25}Mg_{0.25}Ni_{0.25}Zn_{0.25})O$ (medium entropy oxide) significantly decreased the configuration entropy from 1.61 R to 1.39 R which increased the need for post-annealing to obtain single-phase oxide. Co acted as a critically necessary element for HEOs to have a high specific capacity and good cycling stability, whereas Zn or Cu did not substantially influence the reversibility. Removing of Zn changed the oxidation behaviour of the compound from one- to two-step (of NiO and CoO) oxidation process. Therefore, the changes were different for each removed element while the addition of other cations could modulate the electrode performance. Additionally, even in the lithiated condition, the rock-salt was maintained and served as a host structure for the conversion reaction. During lithiation, some cations were reduced and the remaining unreduced cations facilitated the reoccupation of the previously reduced cations to the original sites of the lattice during oxidation. Therefore, during lithiation, the rock-salt structure was preserved and only highly disordered defect-rich regions were present. Upon electrochemical cycling, metal ions were incorporated into the rock-salt structure [151]. This new concept for entropy-stabilized

oxides has the potential to gain completely different properties only by combining a number of possible metals. HEOs substantially differ from classic electrode materials and turn to be very promising materials for reversible electrochemical energy storage.

3.3 Solar cells

The main functions of a solar cell include photogeneration of charge carriers in a material that absorbs light and separation of these carriers to conductive materials that transmit the electricity. Most of the carriers are generated near the surface. When a light quantum falls upon a semiconductor, electron–hole pairs are generated which strongly enhances the conductivity. If their recombination is prevented, they could reach the *p*–*n* junction where the electric field separates the charges.

Metal oxide semiconductors are environmentally friendly, low cost, and highly stable materials. Over the past decade, they have been applied in photovoltaics (PV) as photoelectrodes in dye solar cells (DSCs) and also used to develop metal oxide *p*–*n* junctions [152]. The extraordinary flexible properties and feasibility by modest, low cost and easily scalable methods make metals oxides an exceptional material in new-generation photovoltaics. They have a very large bandgap energy range and are also highly tuneable, thanks to which possibly several metal oxides are more applicable as photo-harvesters. However, silicon (1st generation solar cell) and other III–V semiconductors have factually experienced much more devotion; not entirely but only elite metal oxides have been really studied as photon absorbers. These oxides applied in photovoltaics could be seen as light absorbers, transparent electrodes, transport layers, and special resources with exclusive properties and functionality.

3.3.1 Cu_2O solar cells

Among all MO_x compounds, the copper oxides (Cu–O) are the most prevalent materials to date. The complete bandgap range in between 1.4 and 2.2 eV [153] can be covered from CuO_x by tuning stable binary oxide phases of copper oxides—Cu_2O (cuprous oxide), CuO (tenorite or cupric oxide), and Cu_4O_3 (paramelaconite).

Cuprous oxide (Cu_2O) is a *p*-type semiconductor attractive as photovoltaic material because of its low cost, high absorption coefficient, good mobility, great availability, and nontoxicity. Since 1920, Cu_2O was used as an electronic material, peaked up in the early 1970s. As Schottky (heterojunction) solar cells Cu_2O power conversion efficiency (PCE) was higher than ~ 8% and it was used as a photocathode in photoelectrochemical cells [154]. Schottky barrier solar cell can be fabricated as a back wall or front wall structures (Fig. 4). A back wall Schottky barrier solar cell that offers a great advantage with its mechanical stability and good sensitivity deposits layers on the top of a metal substrate usually by partial thermal oxidation, sputtering, or spray technology. A thin semiconductor layer is needed for light illumination because of its high absorption coefficient and low diffusion length of carriers. When a metal material (Ag, Au, Cu) or carbon (ohmic contacts) is deposited on the rare of the semiconductive layer front wall-type cell is completed [155]. All Schottky barrier solar cell indicated a major part of the potential drop at the metal/cuprous oxide interface (regardless the type of metal used) and only the electrons that could overcome this high-resistance barrier contribute to the external current of the cell. For that reason, the reported

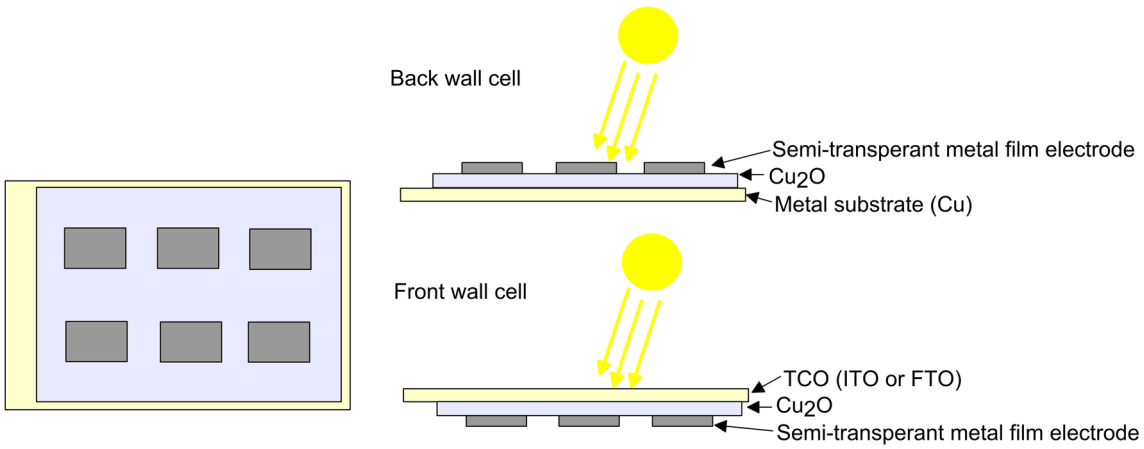

Fig. 4 Schematic representation of Schottky barrier solar cell: face (rare) and profile of the back wall and front wall cell structures. Adapted from [155]

efficiency values were very low. However, by the use of heterojunction, multicomponent oxides based on TCO thin film, in particular, ITO/ZnO/Cu_2O solar cell, displayed the best efficiency of above 2% [156] which is much lower than the theoretical maximum efficiency of Cu_2O equal to about 19–20%.

Homojunction Cu_2O solar cells refer to the structures where the *p–n* junction is composed exclusively of Cu_2O and well-thought-out as one of the methods to enhance the power conversion efficiency of Cu_2O solar cells [157]. The electron affinity of Cu_2O is low compared to many other semiconducting materials. Because of the lattice matching, the strains at the interface should be reduced. Homojunction Cu_2O solar cell had an efficiency of 1.06% because of the high resistivity of *p-/n*-bilayers [158]. In addition, surface sulphidation of electrodeposited *n*-Cu_2O and the *p*-Cu_2O film was found to be useful for improvement in the film photoactivity [159]. It was found out that on the efficiency of homojunction Cu_2O solar cell grain size and crystal orientation had a significant role because of changing the resistivity of the *p*-type Cu_2O [160]. It follows that the methods of synthesis highly influence the performance of the homojunction Cu_2O solar cells. Although prepared by simple methods (such as electrodeposition or spray pyrolysis) using cheap and available materials, Cu_2O films still demonstrate low electrical power conversion efficiency.

3.3.2 Binary heterojunction solar cells

In the *p–n* junction (heterojunction) of two semiconducting materials where one of them displays a higher affinity to electrons whereas the other—to holes, local electric field increasing excitation and current is created. As doping of *n*-type Cu_2O is persistently hindered, a relevant bilayer ZnO oxide either planar [161] or nanostructured [162] was used as oxide window for Cu_2O absorbers. ZnO and Ga_2O_3 display tailored band edge offset applied to Cu_2O. Among *n*-type windows, ZnO is characterized by low-temperature synthesis, inherently low-cost methodology, high electron mobility (~ 120 $cm^2 V^{-1}s^{-1}$), and wide direct bandgap (~ 3.37 eV) [163]. Electrodeposited Cu_2O layers still demonstrate a lower-power conversion efficiency of 1.43% compared to Cu_2O/ZnO solar cells. ZnO (transparent window layer)/Cu_2O solar cell indicated that the dominant current flow mechanism across the heterojunction is the diffusion of holes against the barrier established by the band bending to recombine with electrons trapped in interfacial states [164]. Compared with ZnO, Ga_2O_3/Cu_2O delivered an enhanced performance of 3.97% and 5.38% depending on the deposition method (ALD and PLD, respectively) [165, 166].

The all-transparent solar cell can be attained by the heterojunction MO_x material with a wide energy bandgap for power generation (with visible light transmittance and UV photon absorption). *p*-type NiO/*n*-type ZnO is transparent heterojunction materials that could be obtained by a solid-state sputtering method. A unit cell was responsible to give a record-high conversion efficiency of 6% with a very high current density (2.7 mA cm^{-2}) and open-circuit voltage of 532 mV. This outstanding transparent solar power is duly credited to the complete UV absorption inducing the considerable excitonic effect for ZnO/NiO heterojunction [167]. All the emerging oxides are being thoroughly examined as light absorbers including cobalt (Co–O) and iron (Fe–O) oxides [168]. However, because of the heterojunction, there are always concerns about the existence of lattice mismatch between the layers with different crystal structures or other defects that could induce lower solar cell performance.

3.3.3 Thin-film solar cells

A thin-film (TF) solar cell (second-generation solar cell) is made by depositing photovoltaic material as several thin layers or monolayer on different substrates such as glass, plastic, or metal. Compared to conventional semiconductors, ferroelectric solar cells demonstrate several orders of magnitude higher photovoltaic voltage than the corresponding bandgap of the material and ability to regulate the photovoltaic characteristics by electric field [169] Dharmadhikari reported the first thin-film solar cell based on ferroelectrics in 1982 [170]. Barium titanate ($BaTiO_3$ or BTO) is the most important ferroelectric material for a wide range of applications. Nonetheless, until recent times, the oxygen octahedra ferroelectric thin film from the PZT ($Pb(Zr,Ti)O_3$) family was extensively studied. Many ferroelectric materials such as $Pb(Zr_{1-x}Ti_x)O_3$ and $LiNbO_3$ also exhibit photoelectric and photovoltaic effects under the illumination of visible and near ultraviolet light; but the magnitude of photocurrent and voltage obtained for the device application are far below the photo-electronics requirements.

$BaTiO_3$ thin films have been extensively studied ferroelectric material over the years because of the wide range of applications. Using RF sputtering $BaTiO_3$ layers/films condensed over (100) *p*-Si achieved a thickness of 0.3–0.5 µm. At temperatures above 500 °C, crystalline $BaTiO_3$ films with a tetragonal structure were obtained. The polarization–electric field (P–E) hysteresis loops and a broad peak in the dielectric constant versus temperature curve at Curie point indicate that $BaTiO_3$ films were ferroelectric. An anomalous photovoltaic effect was observed in these thin films which were related to the remnant polarization of the material. The results on open-circuit

and short-circuit measurements provide an important basis for a better understanding of the role of the photovoltaic field, photovoltaic current, and the pyroelectric properties in photoferroelectric domain switching [170]. Although eco-friendly material, $BaTiO_3$ suffers from low thermal stability and loses ferroelectricity at a temperature of about 130 °C because of phase transformation and strain relaxation. When pores were introduced that induced anisotropic strains or heterointerfaces into the nanocomposites of $BaTiO_3$ and $SrTiO_3$, the ferroelectric phase of BTO was stabilized [171]. In another study, to decrease the bandgap of BTO material, Nd-doped $BaTiO_3$ thin films with single tetragonal perovskite phase were sol–gel deposited. When doping with 2 at% Nd, the average grain size slightly increased and after that up to 5 at% Nd the grain sizes decreased with increasing Nd content. The open-circuit photovoltage, power conversion efficiency, and short-circuit photocurrent density reached maximum values at 2 at% Nd because of a change in bandgap and residual polarization [172]. In addition to the history of over 40 years of research, there is still a need for a deeper understanding of the enhanced photoresponse and requirement for developing new materials with improved conductivity, thermal stability, together with reduced bandgap and thickness.

3.3.4 Indium tin oxide

Indium tin oxide (ITO) is one of the most commonly used transparent conducting oxides owing to its two main properties: optical transparency and electrical conductivity. It has high conductivity, hardness, chemical inertness, high work functions (~ 4.8 eV) [173], and transmission of over 80% in the visible range of the solar spectrum. ITO films exhibit also anti-reflection properties and good spectral response in the blue visible region [174]. Like in most transparent conducting films a compromise was made between conductivity and transparency, since increasing both thickness and charge carriers concentration might surge conductivity, but optical transparency drops. For that reason, the thickness of the transparent electrode ITO films ranges from 150 up to 700 nm while below 150 nm the film resistivity increases [175]. Depending on the oxygen content ITO behaved as an alloy or a ceramic but its typical composition is oxygen-saturated containing 74% In, 18% O_2, and 8% Sn by weight. The unsaturated compositions were labelled as oxygen-deficient ITO, which showed to be very transparent and colourless as a thin layer, while its bulk form turned yellowish to grey in colour. In the infrared (IR) region, it performs as a metallic mirror.

ITO is an *n*-type transparent conductive oxide where tin is a dopant in indium oxide lattice. Because of the complex structure of crystalline In_2O_3, it was thought that the factors that determine the high conductive mechanism and lead to a low resistivity were unclear [176]. Recently, it was found that ITO could both donate and accept electrons in dye-coated ITO films when photoinduced charge transfer occurred [177]. When ITO was modified with elements such as Mg, Ca, Yb, etc., the electrodes maintained their electrical characteristics but increased their ambient stability [178]. This optoelectronic material is broadly applied both in research and industry as a thin film in photovoltaics, gas sensors, polymer-based electronics, antennas, and for glass windows to conserve energy [179]. Conventionally used ITO electrodes have a drawback of low resistivity, high transmittance, and high process temperatures for crystallization [180]. Apart from the high cost and energy that vacuum deposition techniques consume, ITO production requires volatile indium incorporation. The film usually indicates brittle nature and low thermal expansion coefficient. As alternatives to ubiquitous ITO, metals, metal oxides, nanomaterial, and polymers are used. ITO/metal/ITO electrodes on plastic or glass substrates are promising candidates for new-generation solar cells that offered the same performance as ITO and more stable mechanical and electric properties while reducing the amount of ITO by four [181].

3.3.5 Amorphous indium–zinc oxide

To lessen indium composition, expurgate working difficulties, and increase electrical homogeneity, amorphous transparent conducting oxides have been developed. Indium zinc oxide (IZO) has some analogous properties to ITO [182]. It is a hole transporting TCO with high work function (5.2 eV) [183]. Warasawa et al. discovered that at a thickness greater than 40 nm, the electrical properties of RF sputtered IZO was independent on film thickness [184]. The crystallization of an amorphous indium zinc oxide is disturbed by the difference in the ratio of oxygen to metal atoms between In_2O_3 and ZnO. The amorphous structure remains unchanged even at 500 °C, thus containing vital processing phases usually seen in organic solar cells. The enhancement within homogeneity improves the usage capability in case of organic solar cells. Additional benefits of IZO are good etchability and higher crystallization temperature than amorphous ITO [185]. By using ALD technique, flexible IZO was fabricated on polyimide substrate by repeated cycles of In_2O_3 and ZnO deposition at three different temperatures—150, 175, and 200 °C. The thin film did not perform degradation, showing great potential to be used for flexible applications [186]. Moreover, together with ITO, doped ZnO films are potential candidates for plasmonic applications [187].

3.3.6 Dye-sensitive solar cells

It was revealed in the late 1960s that organic dyes upon illumination produce electricity at the oxide electrodes in electrochemical cells [188]. A dye-sensitized solar cell (DSSC or DSC, belonging to third-generation solar cell) contains a thick film of semiconductor nanoparticles, a monolayer of organic dye molecules adsorbed to the nanostructured layer, liquid electrolyte (redox shuttle I_3^-/I^-), and counter electrode (Fig. 5). The photoexcited electron in the dye is injected into the conduction band of the semiconducting material (*n*-type DSSC such as TiO_2) and by hopping between the particles, the electron diffuses to the anode. When hopping, the electron could recombine with the electrolyte. When photoexcitation is followed by a hole injection into the conductive band of the semiconductor, the solar cell is *p*-type (for example with NiO electrode material). The recombination limits the efficiency of the DSSC. Usually, *p*-type DSSCs had lower performance than *n*-type DSSCs because of lack of suitable wide bandgap semiconductor with good charge transport properties and sufficient transparency [189]. A later version of a dye solar cell was known as Grätzel cell.

As the dye molecules are quite small, the MONPs are used as 3D scaffolds to hold a large number of dye molecules at a given surface area of the cell. Most of the researchers mainly focus on maximizing the conversion efficiency by improving the molecular design, light-harvesting assemblies, or developing of new hierarchical nanostructures. For example, 3D nanowire-based DSSC with a structure like "caterpillar" indicated a significant improvement in the amount of light absorbed because of the enhanced total surface area leading to higher shortcut circuit currents [190]. The overall power conversion efficiency was measured to be as high as 5.2%. Another study reports the fabrication of highly efficient solid-state DSSCs composed of multilayer TiO_2-coated ZnO nanowire arrays as photoanodes [191]. The straight channels in the hole transporting material allowed a multistep filling process of the 50-μm-thick sensitized film. Its average power conversion efficiency was equal to 5.65%. Recently, hybrid (dye-sensitized and quantum dots (QDs)) solar cells have been presented. When vertically aligned polymer-TiO_2 nanorod arrays were modified with $CuInS_2$-QDs interpenetrating the channels of the nano-oxide, much larger photocurrent and thereby efficiency was observed [192]. This effect was attributed to the combined contribution of QDs absorption in the visible spectrum and the strong interaction and additional interfaces of $CuInS_2$-polymer-TiO_2 for excitation dissociation and charge transfer. Another strategy for the improvement in DSSCs performance includes the use of doped materials with higher conduction band energy. The photoelectric conversion efficiency of DSSCs based on 1 mol% Sn-doped TiO_2 electrode achieved 8.13% which is high than the undoped DSSCs (7.36%) [193]. Despite the good electronic properties of MONPs, the oxidation by holes (generated through band gap excitation) of the redox species in the electrolyte leads to photocorrosion that may affect the performance of the semiconductor. Nonetheless, employing different designs, the architecture of cells, and materials for light absorption, DSSCs provide various opportunities for tuning the performance of the solar cell.

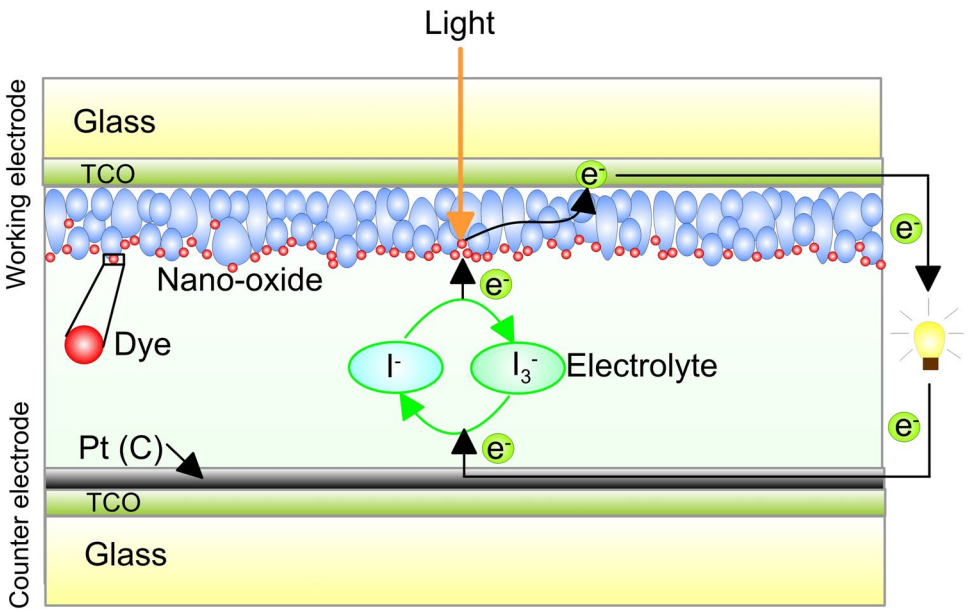

Fig. 5 Scheme of the structure and operating principle of a DSSC device. The electrode nano-oxide layer is covered by dye molecules that absorb solar energy. TCO facilitates charge transfer to the counter electrode layer usually made by Pt or C. Iodide electrolyte supplies electrons to dye molecules that have delivered electrons to nano-oxide particles when being excited

3.4 Antennas

Antenna converts electromagnetic radiation in space into electrical current. The main idea of an antenna is to conduct electricity (as radio waves are one form of electricity), so it is certain that antenna must have conductivity and should not get oxidized. Traditionally rigid materials such as pure metals are the best conductors, but most of the metals are susceptible to oxidation in several ways. When a pure metal is exposed to air, oxidation starts—silver and copper turn into oxides while gold hardly oxidizes at all but the cost is also a vital parameter. Plain iron rusts out pretty hastily. Aluminium oxide is a remarkably stable thin grey layer over aluminium that doesn't really have an effect on its conductivity. Obviously, some conductive materials achieve useful electrical antenna parameters but they are non-transparent and are hardly integrated on flexible carriers.

The best way to overcome this is to call upon metal oxides that are stable enough to be used as antennas. They seem to be an alternate source as antenna materials. Vanadium dioxide (VO_2) is a "smart material" that can make suddenly transition from an insulator to a conductor or the so-called reversible semiconductor–metal phase transition from a monoclinic insulating phase to a tetragonal metallic crystal structure at 66.85 °C. A fast-phase transformation could be triggered by an electric field, terahertz signals, mechanical stress, light, etc. For that reason, researchers have deposited a series of gold resonators on the vanadium dioxide and registered the insulator–metal transition (IMT) towards a controlled electric field [194]. Additionally, composites containing VO_2 demonstrated the possibility of varying widely their electrical and optical properties. Consequently, other researcher group deposited a thin film of VO_2 between a substrate of sapphire (another form of Al_2O_3 (corundum), non-conductive and tolerant of high heat) and a patchwork of gold resonators with sizes equal to 76 × 76 µm separated by 25 µm. When combined Au and VO_2 acted as a *metamaterial,* a substance not found in nature, but capable of manipulating electromagnetic waves were designed to behave in a controlled way [195].

3.4.1 Optically transparent antennas (microstrip, patch)

The fast development of wireless resonance frequency and microwave communication systems increases the demands for construction of reduced size, low cost, low weight, and mechanically robust microstrip antenna with application in vehicles, rockets, planes, satellites, radars, etc. An optically transparent antenna contains primarily a radiation patch (usually with a rectangular shape) above the transparent glass substrate and a frequency selective surface acting as a ground plane for microstrip antenna on the glass rear side (Fig. 6). The radiation in the patch antenna occurs at the open-circuit edges where the electric field extends and fringing fields exist because of the low values of dielectric constant (ε) of the substrate. As seen in Fig. 6, the electric field varies along the patch length and is equal to zero at the centre of the patch.

The patch radiates linearly polarized waves. The size of the patch is reversely proportional to the frequency. For its size reduction, different approaches such as changing antenna geometry, fractal geometry, or dielectric loading could be used. For example, when fractal and geometric designs in antenna substrates are used for specific applications, the antenna performance could be improved by a few orders [196]. The interaction between the patch and the ground plane occurs in the substrate in between. The higher the relative permittivity of the dielectric substrate, the narrower the bandwidth and lower the efficiency. This is due to the fact that the electric field remains in the substrate and does not radiate. For miniaturizing microstrip patch antenna, using nanotechnology techniques nanomagnetic particles (such as nanocrystallite $Mn_{0.5}Zn_{0.3}Co_{0.2}Fe_2O_4$ and $BaFe_{12}O_{19}$ particles) were added into dielectric materials to obtain magneto-dielectric substrates that are less capacitive when opposed to high permittivity materials [197].

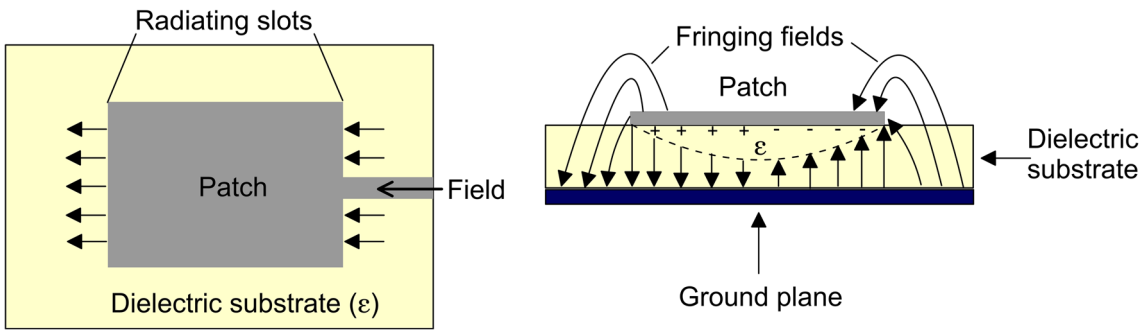

Fig. 6 Top and side view of the geometry of a microstrip patch antenna and its radiation mechanism. The fringing field between the periphery of the patch and ground plane is a function of the dimension of the patch and the substrate height

Lately, transparent conducting materials (TCM) have begun to expose themselves as a serious constituent for emerging optically transparent electronic components like organic light-emitting diodes (OLED), liquid crystal displays (LCD) [198], solar cells [199] and optical antennas [200]. An optically transparent antenna can be integrated on the surface of multifunctional devices reducing the occupied area and resources used [201]. For example, a unique advantage of optically transparent antennas is that they could be integrated on a solar cell without affecting the appearance of products [202] or could be mounted on the optical display to facilitate the reduction in overall system size. We designed another microstrip patch antenna (MPA) on photonic bandgap structures which was optically transparent. Microstrip patch antenna's radiation features were calculated and investigated in the visible region of the spectrum. The designed antenna consisted of ITO used both as a radiating patch and a ground plane parted by a thin (5 µm) glass substrate [203].

Terahertz (THz) radiation is a long wavelength electromagnetic spectra absorbed by the earth's atmosphere. It is applied in useful applications like imaging, sensing, spectroscopy, indoor networking wireless systems, weapon screening, explosives, etc. Our research group constructed terahertz optically transparent E-shaped patch antenna consisting of a radiating patch and a ground plane both made of transparent indium oxide film doped with Ti and parted by a thin polyimide substrate. Its radiation performance examined amid 710–785 GHz band indicated a gain of more than 2.6 dB and the impedance bandwidth of 10% [204]. Other research group analysed the radiation performance in the 705–804 GHz band of optically transparent E-shaped patch antenna based on fluorine-doped tin oxide (FTO). Initially, the designed antenna was simulated by ANSYS: high-frequency electromagnetic field simulation (HFSS), which is a 3D electromagnetic (EM) simulation software mainly used for designing and simulating high-frequency (HF) electronic products such as antennas, microwave and RF components, filters, connectors, etc. and for calculating features like radiation efficiency, gain, impedance bandwidth, directivity, etc. The results obtained showed that the transparent patch antenna of fluorine-doped SnO_2 (FTO) overwhelmed the restrictions of some conventional patch antenna and could be employed for solar cell antenna in satellite systems [205]. To authenticate the feasibility at the ultrahigh frequency (UHF) band, a transparent monopole antenna containing an ITO/Cu/ITO film with an R_s of 4.7 Ω/sq was printed on a glass substrate. The thickness of the layers was equal to 85 (ITO), 13 (Cu), and 85 nm (ITO) and the maximum optical transmittance was 61%. In contrast to a gain of 4.10 dB for the ITO film, the multilayered film featured a hypothetical gain of − 1.96 dB [206].

So far, optically transparent antennas have been studied for more than a decade. The study of these materials makes transparent antennas very comprehensive whereas extensive applications of optically transparent antennas in the real world attract them more attention. A case in point would be an optically transparent GPS antenna integrated into the windshield of a car [207] and the optically transparent RFID reader antenna for smart fitting room application [208].

Optically transparent antennas at present are available in four kinds:

(a) A *metal oxide* film (for e.g. ITO film)—within the antenna design, a compromise must be made between the light transmittance and surface impedance [209];
(b) *Multilayer silver-coated* polyester thin film (such as AgHT series)—compared with ITO film, the AgHT film has better conductivity and worse transmittance [210];
(c) An *ultrathin metal film* made of Cu, Ag, Au, and other metal conductors—such antennas have high radiation efficiency and pretty low light transmittance [211];
(d) *Metal mesh antenna* it demonstrates the highest radiation efficiency and light transmittance higher than that of the ultrathin metal film. However, it has high requirements for processing technology [212, 213].

ITO films are the most widely used materials in the research and design of optically transparent antennas and considering the light transmittance, conductivity, and processing technology of the four materials, ITO films are the best choice. However, a disadvantage of the brittle polycrystal ITO is its higher surface resistance because of the losses in conductivity resulting in lower efficiency.

The MONPs have future usage in electronics, electromagnetic, and microwave applications, as they have been estimated for high-frequency prospective antenna applications and dual function as an antenna and focusing lens for solar cells [214]. The progress in the growth of novel tailorable dielectric materials by deposition of metal or metal oxide nanoparticles on carbon nanotubes (CNTs) using a solvent-free method (which is green, rapid and scalable), permitted CNTs to align or decorate with nm dimensions the polymer matrix [215]. This enables the fabrication not only of transparent but also flexible devices. The tailorable complex permittivity parameters improved the dielectric constant while the loss factor was diminished. Additionally, by changing the amount of metal or MONPs bound to the substrate surface, the discontinuation midst, dielectric constant, and loss factor could be governed [216].

3.4.2 Rectifier (rectenna)

With increasing global demand for enduring choice of renewable energy resources, better harvesting solar radiation devices that will quickly shrink fossil fuel reserves are needed. Because some solar cell efficiency is limited, alternative solar energy converters are attracting attention. Rectenna devices absorb effectively the propagating and oscillating magnetic and electric fields of solar radiation. The rectifier converts the input AC signals from the electromagnetic waves to a usable DC signal that could be transferred to load [217]. Usually, the device performance is limited by the cutoff frequency of the diode and impedance matching between rectifier and antenna. THz antenna combined with a rectenna (rectifier) for garnering IR energy could be used not only for a light-harvesting purpose but also as a photodetector. As Schottky diodes are not able to rectify at the high terahertz region, metal–insulator–metal (MIM) diodes are being considered. The most important shortcoming of a THz rectifier with good rectification concerns their ability to have a higher resistance (megaohms). To achieve high electron affinity insulator, a proper insulator with a small thickness and a large dielectric constant should be selected. Researchers provide an improved alternative resonant bowtie antenna to bring out highly boosted localized fields found at bow tip. In order to profit from this augmentation, the rectifier is produced between the overlapped antenna s-arms using a 0.7 nm copper oxide (CuO) having a relative permittivity of 2.4 at 28.3 THz [218]. A MIM diode produced by electron beam lithography had a smaller contact area (67×67 nm) in order to reduce its capacitance while the oxide layer was thin enough (0.7 nm) to provide a decrease in its resistance. The thin-film-based diode offers a comparatively low zero bias resistance of 500 Ω, thus refining the matching impedance with that of the antenna. To obtain high responsivity and low resistance, Grover et al. designed multi-insulator (metal–insulator–insulator–metal—MIIM) diodes demonstrating improved performance. Comparing asymmetric MIM (NbN–Nb_2O_5–Nb) with thick and thin MIIM diodes (W-Nb_2O_5 (3 nm)-Ta_2O_5 (1 nm)-W, (MIIM 1), and W-Nb_2O_5 (1 nm)-Ta_2O_5 (1 nm)-W, (MIIM 2)) under negative bias, a sharp increase in current for MIIM 2 diode led to higher responsibility and lower resistance. Both multi-insulator diodes provided low resistance and substantial nonlinearity either because of resonant tunnelling or a step change in tunnelling distance with voltage [219].

3.5 Optoelectronic and electronics

3.5.1 *P*-type transparent conducting oxide

Amid numerous oxide materials available, the utmost significant oxide-based material which creates maximum attention for materials scientists is semiconducting transparent films: better known as transparent conducting oxides (TCOs). As special solitary materials, TCOs combine optical transparency with electrical conductivity. Because of their unique properties, they are intended to be extensively utilized for essential aspects of long-standing applications in optoelectronics industries [220, 221] as solar cells production, but also for flat panel displays, LEDs, touch screens, low-emissivity windows, etc. Most of the available TCOs such as F-doped SnO_2 (FTO) or Sn-doped In_2O_3 is *n*-type while obtaining functional *p*-TCOs still remains a considerable challenge. Because of the increasing Indium cost, extensive research is undertaken to obtain hole-conducting fully transparent counterparts that could replace In-rich TCOs. Presently, a majority portion of the research in *p*-TCO technology was focused on the production of high-quality films for a device with far greater electrical parameters. Some authors explained the hindered development of efficient *p*-type TCOs with the highly localized nature of the O 2*p* derived valence band that causes difficulties in introducing shallow acceptors and large hole effective masses [222]. The localized around the oxygen atom pores require high energy for migration within the lattice and, therefore, low pore mobility and electric conductivity are present. Recently, Cu-containing *p*-type TCOs such as $M^{II}\ Cu_2O_2$ (M^{II}—bivalent ions like Mg, Ca, Sr, Ba) and $CuM^{III}\ O_2$/(M^{III}—trivalent ions such as Al, Ga, In) have been proposed [223]. When divalent cation replaced trivalent, in the valence band an empty state that acted as a hole and increased conductivity, was created. For example, when Sr^{2+} substituted La^{3+} in $La_{1-x}Sr_xVO_3$ compounds high concentration of hole carriers at the top of the valence band occurred. These *p*-type TCOs films made of $La_{2/3}Sr_{1/3}VO_3$ demonstrated weak absorption in the visible region, the highest transmission between 53.9 and 70.1% in the visible region, modest carrier mobility, and the highest conductivity in the range 742.3–872.3 S cm^{-1} at RT. Therefore, the good balance between optical transparency and electrical conductivity in the delafossite compound led to these high figures of merit as compared with other developed *p*-type TCOs [224]. It follows that *p*-TCO thin films deposited by co-doping could propose better optical, electrical properties combined with maximum conductivity without interfering with their visible transmittance.

Summary and prospects

Metal oxide nanoparticles became significant components in applied nanotechnology for trace gas sensors, batteries, magnetic storage media, solar cells, catalysis, energy conversion, architecture, medicine, food, agriculture, cosmetics, textile, antennas (including microstrip and patch-type

optically transparent antennas), rectifiers; optoelectronic and electronics clearly enhance the performances in terms of sensitivity and detection limits down to single molecules detection. The principles, advantages, and disadvantages of various semiconductor gas sensors, antennas, solar cells, batteries, etc. were explained and compared in order to find new strategies in designing such nanomaterials in functional devices. Metal oxide nanoparticles with their nanoarchitecture and hierarchical structure are proved to be valuable substances to design gas sensors with excellent selectivity, fast sensing response, and recovery. The performance of existing commercially available gas sensors can be further improved by having greater control over the microstructure, size of NPs, and their composition. Further, a combination of different nanomaterials could increase the performance of the functional device.

In terms of challenges posed by MONPs used in nanotechnology, the design and synthesis of novel, robust and flexible nano-oxides with high sensitivity, excellent selectivity, reduced size, expanded lifetimes, and fast response in a wide range of applications and environments is an important trend in the field of gas sensors. However, more efforts should be focused towards the proper selection of type, morphology, design of hierarchical structures of nano-oxides as well as the optimal composition of additives that display the best performance for detection of a particular environmental reductant, oxidant, or VOCs gas. Although nowadays metal oxide sensors have limited commercial use, the new MONPs developed possess unique properties at a relatively low cost which gives encouraging results for many sensing applications.

With regard to light harvesting, as the efficiency of quantum devices is limited by the bandgap energy of the nano-oxide layer, the energy could be lost either because of the low energy of the passing photons or in form of heat from high-frequency photons. The upconversion of the nanostructures in the broad spectral range under sun irradiance is required. Therefore, multiple excitation generations and band gap tenability that has a direct influence on photon adsorption and the generation of photocurrent is of prime importance. It is essential to building solar harvesting devices based on optimized design and technology and unforeseen opportunities are to be pursued in the near future.

On the other hand, the modern wireless communication systems need solutions for changing narrow bandwidth with multiband antennas with better radiation, high data rate, and highly miniaturized. The appealing future scopes on transparent and flexible devices with high optical transmittance in the infrared region and working in 4G, 5G, or PSC frequency range.

As nanotechnologies mature, different applications of MONPs appear including energy conversion, optical imaging, data storage, antennas, etc. Because of the huge number of different nano-oxides and their specific properties, only principle advantages of some MONPs are given herein. The scientific and technical works show that the importance of nanotechnology improvement increases at a rapid pace and this review could be helpful for researchers working on devices with novel designs.

Author's contribution MPN and MSC conceived of the presented idea and carried out a detailed review. MSC designed and supervised the whole work. In manuscript planning, articulation, the majority writing part was done by MPN with inputs and a substantial contribution from MSC. Authors equally contributed to the work related to illustrations and tables. Also, both MPN and MSC thoroughly discussed the contents, results and commented on the design of the figures, parameters in the tables, and completed the final manuscript review.

Funding MSC acknowledges the research grants from the Department of Science and Technology (DST), Government of India for the three major R&D projects: (a) SR/FTP/CS-116/2007, (b) No. SR/FT/CS134/2010, and (c) No. GITA/DST/TWN/P-002/2009 and Ministry of Science and Technology (MOST), Republic of China (Taiwan) for its constant support through research grants, travel grants, and many others.

Compliance with ethical standards

Conflict of interest The authors declare that they have no conflict of interest.

Human and animal rights This chapter does not contain any studies with human participants or animals performed by any of the authors.

References

1. Castro-Alarcón N, Herrera-Arizmendi JL, Marroquín-Carteño LA, Guzmán-Guzmán IP, Pérez-Centeno A, Santana-Aranda MÁ (2016) Antibacterial activity of nanoparticles of titanium dioxide, intrinsic and doped with indium and iron. Microbiol Res Int 4(4):55–62
2. Bindhu MR, Umadevi M, Kavin Micheal M, Arasu MV, Al-Dhabi NA (2016) Structural, morphological and optical properties of MgO nanoparticles for antibacterial applications. Mater Lett 166:19–22. https://doi.org/10.1016/j.matlet.2015.12.020
3. Khashan KS, Sulaiman GM, Abdulameer FA (2016) Synthesis and antibacterial activity of CuO nanoparticles suspension induced by laser ablation in liquid. J Sci Eng 41:301–310. https://doi.org/10.1007/s13369-015-1733-7
4. Music S, Dragcevic D, Maljkovic M, Popovic S (2003) Influence of chemical synthesis on the crystallization and properties of zinc oxide. Mater Chem Phys 77:521–530. https://doi.org/10.1016/S0254-0584(02)00088-3
5. Wilson N (2018) Nanoparticles: environmental problems or problem solvers? Bioscience 68(4):241–246. https://doi.org/10.1093/biosci/biy015
6. Marquis G, Ramasamy B, Banwarilal S, Munusamy AP (2016) Evaluation of antibacterial activity of plant-mediated CaO nanoparticles using *Cissus quadrangularis* extract. J Photochem

Photobiol B 155:28–33. https://doi.org/10.1016/j.jphotobiol.2015.12.013
7. Taylor R, Coulombe S, Otanicar T, Phelan P, Gunawan A, Lv W, Rosengarten G, Prasher R, Tyagi H (2013) Small particles, big impacts: a review of the diverse applications of nanofluids. Appl Phys 113:011301. https://doi.org/10.1063/1.4754271
8. Bansal V, Poddar P, Ahmad A, Sastry M (2006) Room-temperature biosynthesis of ferroelectric barium titanate nanoparticles. J Am Chem Soc 128:11958–11963. https://doi.org/10.1021/ja063011m
9. Liu W-T (2006) Nanoparticles and their biological applications. J Biosci Bioeng 102:1–7. https://doi.org/10.1263/jbb.102.1
10. Poole CP Jr, Owens FJ (2003) Introduction to nanotechnology. Wiley, Hoboken
11. Lang C, Schuler D, Faivre D (2007) Synthesis of magnetite nanoparticles for bio-and nanotechnology: genetic engineering and biomimetics of bacterial magnetosomes. Macromol Biosci 7:144–151. https://doi.org/10.1002/mabi.200600235
12. Jun Y-W, Seo J-W, Cheon J (2008) Nanoscale laws of magnetic nanoparticles and their applicability in biomedical sciences. Acc Chem Res 41:170–189. https://doi.org/10.1021/ar700121f
13. Klem MT, Resnick DA, Gilmore K, Young M, Idzerda YU, Douglas T (2007) Synthetic control over the magnetic moment and exchange bias in all-oxide materials encapsulated within a spherical protein cage. J Am Chem Soc 129:197–201. https://doi.org/10.1021/ja0667561
14. Franke ME, Koplin TJ, Simon U (2006) Metal and metal oxide nanoparticles in chemiresistors: does the nanoscale matter? Small 2(3):36–50. https://doi.org/10.1002/smll.200500261
15. Sansonov GV (1982) The oxide handbook. IFI/Plenum Press, New York
16. Yahiro J, Oaki Y, Imai H (2006) Biomimetic synthesis of wurtzite ZnO nanowires possessing a mosaic structure. Small 2:1183–1187. https://doi.org/10.1002/smll.200600214
17. Mejias JA, Marquez AM, Fernandez-Sanz J, Fernandez-Garcia M, Ricart JM, Sousa C, Illas F (1995) On modelling the interaction of CO on the MgO (100) surface. Surf Sci 327:59–73. https://doi.org/10.1016/0039-6028(94)00831-0
18. Margaryan AA, Liu W (1993) Prospects of using germanium-dioxide-based glasses for optics. Opt Eng 32:1995–1996
19. Lee S-Y, Gao X, Matsui H (2007) Biomimetic and aggregation-driven crystallization route for the room-temperature material synthesis: the growth of β-Ga_2O_3 nanoparticles on peptide assemblies as nanoreactors. J Am Chem Soc 129:2954–2958. https://doi.org/10.1021/ja0677057
20. Klem MT, Mosolf J, Young M, Douglas T (2008) Photochemical mineralization of europium, titanium, and iron oxyhydroxide nanoparticles in the ferritin protein cage. Inorg Chem 47:2237–2239. https://doi.org/10.1021/ic701740q
21. Zhang W, Zhang D, Fan T, Ding J, Guo Q, Ogawa H (2006) Fabrication of ZnO microtubes with adjustable nanopores on the walls by the templating of butterfly wing scales. Nanotechnology 17:840–844. https://doi.org/10.1088/0957-4484/17/3/038
22. Aizenberg J, Hanson J, Koetzle TF, Weiner S, Addadi L (1997) Control of macromolecule distribution within synthetic and biogenic single calcite crystals. J Am Chem Soc 119:881–886. https://doi.org/10.1021/ja9628821
23. Biro LP, Balint Z, Kertesz K, Vertesy Z, Mark GI, Tapaszto L, Vigneron JP, Lousse V (2007) Photonic crystal structures of biologic origin: butterfly wing scales. Mater Res Soc Symp Proc 1014, AA07-08-16
24. Zou D, Xu C, Luo H, Wang L, Ying T (2008) Synthesis of Co_3O_4 nanoparticles via an ionic liquid-assisted methodology at room temperature. Mater Lett 62:1976–1978. https://doi.org/10.4236/snl.2012.21001
25. Wilkes JS, Zaworotko MJ (1992) Air and water stable 1-ethyl-3-methylimidazolium based ionic liquids. Chem Commun 13:965–967. https://doi.org/10.1039/C39920000965
26. Nuraje N, Su K, Haboosheh A, Samson J, Manning EP, Yang N-l, Matsui H (2006) Room temperature synthesis of ferroelectric barium titanate nanoparticles using peptide nanorings as templates. Adv Mater 18:807–811. https://doi.org/10.1021/ja063011m
27. Liu X, Zhang J, Wu S, Yang D, Liu P, Zhang H, Wang S, Yao X, Zhu G, Zhao H (2012) Single crystal α-Fe_2O_3 with exposed 104 facets for high-performance gas sensor applications. RSC Adv 2:6178–6184
28. Li X, Wei W, Wang S, Kuai L, Geng B (2011) Single-crystalline α-Fe_2O_3 oblique nano parallelepipeds: high-yield synthesis, growth mechanism and structure enhanced gas-sensing properties. Nanoscale 3:718–724. https://doi.org/10.1039/C0NR00617C
29. Ayesh AI, Abu-Hani AFS, Mahmoud ST, Haik Y (2016) Selective H_2S sensor based on CuO nanoparticles embedded in organic membranes. Sens Actuators B Chem 231:593–600. https://doi.org/10.1016/j.snb.2016.03.078
30. Haija MA, Ayesh AI, Ahmed S, Katsiotis MS (2016) Selective hydrogen gas sensor using $CuFe_2O_4$ nanoparticle-based thin film. Appl Surf Sci 369:443–447. https://doi.org/10.1016/j.apsusc.2016.02.103
31. Gadkari AB, Shinde TJ, Vavambekar PN (2011) Ferrite gas sensors. IEEE Sens J 11(4):849–861. https://doi.org/10.1109/JSEN.2010.2068285
32. Korotcenkov G, Cho BK (2017) Metal oxide composites in conductometric gas sensors: achievements and challenges. Sens Actuator B Chem 244:182–210. https://doi.org/10.1016/j.snb.2016.12.117
33. Sun Y-F, Liu S-B, Meng F-L, Liu J-Y, Jin Z, Kong L-T, Liu J-H (2012) Metal oxide nanostructures and their gas sensing properties: a review. Sensors (Basel) 12(3):2610–2631. https://doi.org/10.3390/s120302610
34. Wang B, Zhu LF, Yang YH, Xu NS, Yang GW (2008) Fabrication of a SnO_2 nanowire gas sensor and sensor performance for hydrogen. J Phys Chem C 112:6643–6647. https://doi.org/10.1021/jp8003147
35. Kuang Q, Lao CS, Wang ZL, Xie ZX, Zheng LS (2007) High-sensitivity humidity sensor based on a single SnO_2 nanowire. J Am Chem Soc 129:6070–6071. https://doi.org/10.1021/ja070788m
36. Ying Z, Wan Q, Song ZT (2004) SnO_2 nanowhiskers and their ethanol sensing characteristics. Nanotechnology 15:1682–1684. https://doi.org/10.1088/0957-4484/15/11/053
37. Wang HT, Kang BS, Ren F, Tien LC, Sadik PW, Norton DP, Pearton SJ, Lin JS (2005) Hydrogen-selective sensing at room temperature with ZnO nanorods. Appl Phys Lett 86:243503. https://doi.org/10.1063/1.1949707
38. Lupan O, Chai G, Chow L (2008) Novel hydrogen gas sensor based on single ZnO nanorod. Microelectron Eng 85:2220–2225. https://doi.org/10.1016/j.mee.2008.06.021
39. Xu JQ, Chen YP, Shen JN (2008) Ethanol sensor based on hexagonal indium oxide nanorods prepared by solvothermal methods. Mater Lett 62:1363–1365. https://doi.org/10.1016/j.matlet.2007.08.054
40. Xu PC, Cheng ZX, Pan QY, Xu JQ, Xiang Q, Yu WJ, Chu YL (2008) High aspect ratio In_2O_3 nanowires: synthesis, mechanism and NO_2 gas-sensing properties. Sens Actuator B 130:802–808. https://doi.org/10.1016/j.snb.2007.10.044
41. Wang CH, Chu XF, Wu MW (2006) Detection of H_2S down to ppb levels at room temperature using sensors based on ZnO nanorods. Sens Actuator B 113:320–323. https://doi.org/10.1016/j.snb.2005.03.011

42. Zhang N, Yu K, Li Q, Wan Q (2008) Room-temperature high-sensitivity H_2S gas sensor based on dendritic ZnO nanostructures with macroscale in appearance. J Appl Phys 103:104305. https://doi.org/10.1063/1.2924430
43. Rout CS, Hegde M, Rao CNR (2008) H_2S sensors based on tungsten oxide nanostructures. Sens Actuator B 128:488–493. https://doi.org/10.1016/j.snb.2007.07.013
44. Kaur M, Jain N, Sharma K, Bhattacharya S, Roy M, Tyagi AK, Gupta SK, Yakhmi JV (2008) Room-temperature H_2S gas sensing at ppb level by single crystal In_2O_3 whiskers. Sens Actuator B 133:456–461. https://doi.org/10.1016/j.snb.2008.03.003
45. Liu J, Li S, Zhang B, Wang Y, Gao Y, Liang X, Wang Y, Lu GJ (2017) Flower-like In_2O_3 modified by reduced graphene oxide sheets serving as a highly sensitive gas sensor for trace NO_2 detection. Colloid Interface Sci 504:206–213. https://doi.org/10.1016/j.jcis.2017.05.053
46. Choi YJ, Hwang IS, Park JG, Choi KJ, Park JH, Lee JH (2008) Novel fabrication of a SnO_2 nanowire gas sensor with high sensitivity. Nanotechnology. https://doi.org/10.1088/0957-4484/19/9/095508
47. Park S, An S, Ko H, Jin C, Lee C (2012) Synthesis of nanograined ZnO nanowires and their enhanced gas sensing properties. ACS Appl Mater Interfaces 4(7):3650–3656. https://doi.org/10.1021/am300741r
48. Li T-T, Bao N, Geng A-F, Yu H, Yang Y, Dong X-T (2018) Study on room temperature gas-sensing performance of CuO film-decorated ordered porous ZnO composite by In_2O_3 sensitization. R Soc Open Sci 5:171788. https://doi.org/10.1098/rsos.171788
49. Liu ZF, Yamazaki T, Shen Y (2007) Room temperature gas sensing of p-type TeO_2 nanowires. Appl Phys Lett 90:173119. https://doi.org/10.1063/1.2732818
50. Kim YS, Hwang IS, Kim SJ (2008) CuO nanowire gas sensors for air quality control in the automotive cabin. Sens Actuator B 135:298–303. https://doi.org/10.1016/j.snb.2008.08.026
51. Guo Z, Li ML, Liu JH (2008) Highly porous CdO nanowires: preparation based on hydroxy- and carbonate-containing cadmium compound precursor nanowires, gas sensing and optical properties. Nanotechnology 19:245611
52. Kim ID, Rothschild A, Lee BH, Kim DY, Jo SM, Tuller HL (2006) Ultrasensitive chemiresistors based on electrospun TiO_2 nanofibers. Nano Lett 6:2009–2013. https://doi.org/10.1021/nl061197h
53. Liu Z, Yu L, Guo F, Liu S, Qi L, Shan M, Fan X (2017) Facial development of high-performance room temperature NO_2 gas sensors based on ZnO nanowalls decorated rGO nanosheets. Appl Surf Sci 423:721–727. https://doi.org/10.1016/j.apsusc.2017.06.160
54. Meier DC, Semancik S, Button B, Strelcov E, Kolmakova A (2007) Coupling nanowire chemiresistors with MEMS micro-hotplate gas sensing platforms. Appl Phys Lett 91:63118–63120. https://doi.org/10.1063/1.2768861
55. Chen Y, Zhang W, Wu Q (2017) A highly sensitive room-temperature sensing material for NH_3: SnO_2-nanorods coupled by rGO. Sens Actuator B 242:1216–1226. https://doi.org/10.1016/j.snb.2016.09.096
56. Zhao YM, Zhu YQ (2009) Room temperature ammonia sensing properties of $W_{18}O_{49}$ nanowires. Sens Actuator B 137:27–31. https://doi.org/10.1016/j.snb.2009.01.004
57. Meng F, Zheng H, Sun Y, Li M, Liu J (2017) Trimethylamine sensors based on Au-modified hierarchical porous single-crystalline ZnO nanosheets. Sensors (Basel) 17(7):1478. https://doi.org/10.3390/s17071478
58. Wang T, Sun Z, Huang D, Yang Z, Ji Q, Hu N, Yin G, He D, Wei H, Zhang Y (2017) Studies on NH_3 gas sensing by zinc oxide nanowire-reduced graphene oxide nanocomposites. Sens Actuator B 252:284–294. https://doi.org/10.1016/j.snb.2017.05.162
59. Kim YS, Hwang IS, Kim SJ (2008) CuO nanowire gas sensors for air quality control in the automotive cabin. Sens Actuator B 135:298–303. https://doi.org/10.1016/j.snb.2008.08.026
60. Zhang D, Jiang C, Liu J, Cao Y (2017) Carbon monoxide gas sensing at room temperature using copper oxide-decorated graphene hybrid nanocomposite prepared by layer-by-layer self-assembly. Sens Actuators B 247:875–882. https://doi.org/10.1016/j.snb.2017.03.108
61. Ramírez FH, Tarancón A, Casals O, Arbiol AJ, Rodríguez R, Morante JR (2007) High response and stability in CO and humidity measures using a single SnO_2 nanowire. Sens Actuator B 121:3–17. https://doi.org/10.1016/j.snb.2006.09.015
62. Van NH, Kim HR, Ju BK, Lee JH (2008) Enhanced performance of SnO_2 nanowires ethanol sensor by functionalizing with La_2O_3. Sens Actuator B 133:228–234. https://doi.org/10.1016/j.snb.2008.02.018
63. Singh N, Gupta RK, Lee PS (2011) Gold-nanoparticle-functionalized In_2O_3 nanowires as CO gas sensors with a significant enhancement in response. ACS Appl Mater Interfaces 3:2246–2252. https://doi.org/10.1021/am101259t
64. Rodríguez-Betancourtt V-M, Bonilla HG, Martínez MF, Bonilla AG, Lazaro JPM, Bonilla JTG, González MA, Amador MLO (2017) Gas sensing properties of $NiSb_2O_6$ micro- and nanoparticles in propane and carbon monoxide atmospheres. J Nanomater 8792567, 9. https://doi.org/10.1155/2017/8792567
65. Gaskov A, Rumyantseva M (2009) Metal oxide nanocomposites: synthesis and characterization in relation with gas sensing phenomena. In: Baraton MI (ed) Sensors for environment, health and security. Springer, Dordrecht, pp 3–29
66. Weschler CJ (2000) Ozone in indoor environments: concentration and chemistry. Indoor Air 10:269–288. https://doi.org/10.1034/j.1600-0668.2000.010004269.x
67. Liu X, Cheng S, Liu H, Sha H, Zhang D, Ning HA (2012) Survey on gas sensing technology. Sensors 12:9635–9665. https://doi.org/10.3390/s120709635
68. Chapelle A, Oudrhiri-Hassani F, Presmanes L, Barnabé A, Tailhades P (2010) CO2 sensing properties of semiconducting copper oxide and spinel ferrite nanocomposite thin film. Appl Surf Sci 256(14):4715–4719. https://doi.org/10.1016/j.apsusc.2010.02.079
69. Herrán J, Mandayo GG, Castaño E (2008) Solid-state gas sensor for fast carbon dioxide detection. Sens Actuator B 129(2):705–709
70. Herran J, Mandayo GG, Castano E (2007) Solid state gas sensor for fast carbon dioxide detection. In: Transducers 2007. International solid-state sensors, actuators and microsystems conference. INSPEC Accession Number: 9828639. https://doi.org/10.1109/sensor.2007.4300296
71. Barsan N, Weimar U (2003) Understanding the fundamental principles of metal oxide based gas sensors; the example of CO sensing with SnO_2 sensors in the presence of humidity. J Phys Condens Mater 15(20):R813–R839
72. Comini E, Cristalli A, Faglia G, Sberveglieri G (2000) Light enhanced gas sensing properties of indium oxide and tin dioxide sensors. Sens Actuator B 65(1–3):260–263
73. Can ZY, Narita H, Mizusaki J, Tagawa H (1995) Detection of carbon monoxide by using zirconia oxygen sensor. Solid State Ionics 79:344–348. https://doi.org/10.1016/0167-2738(95)00085-K
74. Zhang D, Sun Y, Jiang C, Yao Y, Wang D-Y, Zhang Y (2017) Room-temperature highly sensitive CO gas sensor based on Ag-loaded zinc oxide/molybdenum disulfide ternary nanocomposite and its sensing properties. Sens Actuator B 253:1120–1128. https://doi.org/10.1016/j.snb.2017.07.173

75. Bandi S, Hastak V, Peshwe DR, Srivastav AK (2018) In-situ TiO_2–rGO nanocomposites for CO gas sensing. Bull Mater Sci 41:115. https://doi.org/10.1007/s12034-018-1632-0
76. Zhang D, Jiang C, Liu J, Cao Y (2017) Carbon monoxide gas sensing at room temperature using copper oxide-decorated graphene hybrid nanocomposite prepared by layer-by-layer self-assembly. Sens Actuator B 247:875–882. https://doi.org/10.1016/j.snb.2017.03.108
77. Takeuchi T (1988) Oxygen sensors. Sens Actuator B 14:109–124
78. Takami A, Matsuura T, Sekiya T, Okawa T, Watanabe Y (1985) Progress in lead tolerant titania exhaust gas oxygen sensors. In: Internation congress on automotive engineering, Detroit, SAE paper 850381, MI, USA
79. Kondo H, Takahashi H, Takeuchi T, Igarashi I (1983) $NbzO_5$ thin-film oxygen sensor. In: Proceedings of 3rd sensor symposium, Tsukuba, Japan, pp 185–190
80. Logothetis EM, Park K, Meitzler AH, Land KR (1975) Oxygen sensors using CoO ceramics. Appl Phys Lett 26:209–211
81. Park K, Logothetis EM (1977) Oxygen sensing with Co_{1-x} Mg_xO ceramics. J Electro Chem Soc 124:1443–1446
82. Yu C, Fukuyama Y, Shimizu Y, Arai H, Seiyama T (1985) Lean burn oxygen sensor using perovskite-type oxides. In: 4th Congress on chemical sensors, Yokohama, Japan, pp 67–68
83. Korotcenkov G, Cho BK (2012) Ozone measuring: what can limit the application of SnO_2-based conductometric gas sensors? Sens Actuator B 161:28–44
84. Knake R, Hauser PC (2002) Sensitive electrochemical detection of ozone. Anal Chim Acta 459:199–207. https://doi.org/10.1016/S0003-2670(02)00121-6
85. Potyrailo RA, Hobbs SE, Hieftje GM (1998) A simple, highly stable scintillator light source for ultraviolet absorption-based sensors. Anal Chim Acta 367:153–157
86. Mori M, Itagaki Y, Sadaoka Y (2012) Effect of VOC on ozone detection using a semiconducting sensor with $SnFe_{1-x}Co_xO_3$ perovskite-type oxides. Sens Actuator B 163:44–50. https://doi.org/10.1016/j.snb.2011.12.047
87. Labidi A, Jacolin C, Bendahan M, Abdelghani A, Guerin J, Aguir K, Maaref M (2005) Impedance spectroscopy on the WO_3 gas sensor. Sens Actuator B 106:713–718. https://doi.org/10.1016/j.snb.2004.09.022
88. Katsarakis N, Bender M, Cimalla V, Gagaoudakis E, Kiriakidis G (2003) Ozone sensing properties of DC-sputtered, c-axis oriented ZnO films at room temperature. Sens Actuator B 96(1–2):76–81
89. Wu R-J, Wu T-M (2010) High sensor response and short response time of ozone sensor using Au/TiO_2–SnO_2 material at room temperature. Sensor Lett 8(4):564–569. https://doi.org/10.1166/sl.2010.1312
90. Wu R-J, Zhu Z, Ji G-D, Wu C-H (2018) Rapid detection of trace ozone by using SWCNT-In_2O_3 materials. Int J Adv Sci Eng Technol 6(2):10–15
91. Wu R-J, Chiu Y-C, Wu C-H, Su Y-J (2015) Application of Au/TiO_2–WO_3 material in visible light photoreductive ozone sensors. Thin Solid Films 574C:156–161. https://doi.org/10.1016/j.tsf.2014.12.009
92. Wu R-J, Lin H-L, Chen M-H, Wu T-M, Chien FS-S (2008) Application of nanostructure ZnO for room working temperature ozone sensor. Sensor Lett 6(6):800–802. https://doi.org/10.1166/sl.2008.504
93. Wu C-H, Jiang G-J, Chiu C-C, Chong P, Jeng C-C, Wu R-J, Chen J-H (2015) A fast gas concentration sensing by analysing the rate of resistance change. Sens Actuator B 209:906–910
94. Wang CY, Becker RW, Passow T, Pletschen W, Köhler K, Cimalla V, Ambacher O (2012) Photon stimulated sensor based on indium oxide nanoparticles. I: Wide-concentration-range ozone monitoring in the air. Sens Actuator B 152:235–240. https://doi.org/10.1016/j.snb.2010.12.014
95. Waitz T, Wagner T, Sauerwald T (2009) Ordered mesoporous In_2O_3: synthesis by structure replication and application as a methane gas sensor. Adv Funct Mater 19(4):653–661. https://doi.org/10.1002/adfm.200801458
96. Vaishampayan MV, Deshmukh RG, Mulla IS (2008) Influence of Pd doping on morphology and LPG response of SnO_2. Sens Actuator B 131(2):665–672
97. Zhang D, Yin N, Xia B (2015) Facile fabrication of ZnO nanocrystalline-modified graphene hybrid nanocomposite toward methane gas sensing application. J Mater Sci Mater Electron 26(8):5937–5945. https://doi.org/10.1007/s10854-015-3165-2
98. Chang B-Y, Wang C-Y, Lai H-F, Wu R-J, Chavali M (2012) Novel nano In_2O_3-WO_3 composite films for ultra trace level (ppb) detection of NO gas at room temperature. Adv Sci Lett 17(1):76–81. https://doi.org/10.1166/asl.2012.4262
99. Chang B-Y, Wang C-Y, Lai H-F, Wu R-J, Chavali M (2014) Evaluation of Pt/In_2O_3-WO_3 nanopowder ultra-trace level NO gas sensor. J Taiwan Inst Chem Eng 45(3):1056–1064. https://doi.org/10.1016/j.jtice.2013.09.002
100. Sahm T, Madler L, Gurlo A, Barsan N (2004) Flame spray synthesis of tin dioxide nanoparticles for gas sensing. Sens Actuator B 98(2–3):148–153. https://doi.org/10.1016/j.snb.2003.10.003
101. Kaur J, Kumar R, Bhatnagar MC (2007) Effect of indium-doped SnO_2 nanoparticles on NO_2 gas sensing properties. Sens Actuator B 126(2):478–484. https://doi.org/10.1016/j.snb.2007.03.033
102. Meng D, Yamazaki T, Shen Y, Liu Z, Kikuta T (2009) Preparation of WO_3 nanoparticles and application to the NO_2 sensor. Appl Surf Sci 256(4):1050–1053. https://doi.org/10.1016/j.apsusc.2009.05.075
103. Reyes LF, Hoe A, Saukko S, Heszler P, Lantto V (2006) Gas sensor response of pure and activated WO_3 nanoparticle films made by advanced reactive gas deposition. Sens Actuator B 117(1):128–134. https://doi.org/10.1016/j.snb.2005.11.008
104. Fan F, Feng Y, Bai S, Feng J, Chen A, Li D (2013) Synthesis and gas sensing properties to NO_2 of ZnO nanoparticles. Sens Actuator B 185:377–382. https://doi.org/10.1016/j.snb.2013.05.020
105. Rai P, Yu Y-T (2012) Citrate-assisted hydrothermal synthesis of single crystalline, ZnO nanoparticles for gas sensor application. Sens Actuator B Chem 173:58–65. https://doi.org/10.1016/j.snb.2012.05.068
106. Jun JH, Yun J, Cho K, Hwang I-S, Lee J-H, Kim S (2009) Necked ZnO nanoparticle-based NO_2 sensors with a high and fast response. Sens Actuator B Chem 140(2):412–417. https://doi.org/10.1016/j.snb.2009.05.019
107. Kolekar TV, Bandgar SS, Shirguppikar SS, Ganachari VS (2013) Synthesis and characterization of ZnO nanoparticles for efficient gas sensors. Arch Appl Sci Res 5(6):20–28
108. Abbasi A, Sardroodi JJ (2016) N-doped TiO_2 anatase nanoparticles as a highly sensitive gas sensor for NO_2 detection: insights from DFT computations. Environ Sci Nano 5:1153–1164. https://doi.org/10.1039/C6EN00159A
109. Liu X, Chen N, Han B, Xiao X, Chen G, Djerdj I, Wang Y (2015) Nanoparticle cluster gas sensor: Pt activated SnO_2 nanoparticles for NH_3 detection with ultrahigh sensitivity. Nanoscale 36:14872–14880. https://doi.org/10.1039/C5NR03585F
110. Zhang D, Jiang C, Li P, Sun Y (2017) Layer-by-layer self-assembly of Co_3O_4 nanorod-decorated MoS_2 nanosheet-based nanocomposite toward high-performance ammonia detection. ACS Appl Mater Interfaces 9(7):6462–6471. https://doi.org/10.1021/acsami.6b15669
111. Zhang D, Liu J, Jiang C, Liu A, Xia B (2017) Quantitative detection of formaldehyde and ammonia gas via metal oxide-modified graphene-based sensor array combining with the neural

network model. Sens Actuator B 240(3):55–65. https://doi.org/10.1016/j.snb.2016.08.085
112. Doeller JE, Isbell TS, Benavides G, Koenitzer J, Patel H, Patel RP, Lancaster JR Jr, Darley-Usmar VM, Kraus DW (2005) Polarographic measurement of hydrogen sulfide production and consumption by mammalian tissues. Anal Biochem 341(1):40–51. https://doi.org/10.1016/j.ab.2005.03.024
113. Gong J, Chen Q, Lian M-R, Liu N-C, Stevenson RG, Adami F (2006) Micromachined nanocrystalline silver doped SnO_2 H_2S sensor. Sens Actuator B Chem 114(1):32–39. https://doi.org/10.1016/j.snb.2005.04.035
114. Vaishampayan MV, Deshmukh RG, Walke P, Mulla IS (2008) Fe-doped SnO_2 nanomaterial: a low-temperature hydrogen sulphide gas sensor. Mater Chem Phys 109(2–3):230–234. https://doi.org/10.1016/j.matchemphys.2007.11.024
115. Devi GS, Manorama S, Rao VJ (1995) High sensitivity and selectivity of a SnO_2 sensor to H_2S. Sens Actuator B 28(1):31–37. https://doi.org/10.1016/0925-4005(94)01535-P
116. Xue X, Xing L, Chen Y, Shi S, Wang Y, Wang T (2008) Synthesis and H_2S sensing properties of CuO–SnO_2 core/shell pn-junction nanorods. J Phys Chem C 112:12157–12160. https://doi.org/10.1021/jp8037818
117. Patil LA, Patil DR (2006) Heterocontact type CuO-modified SnO_2 sensor for the detection of a ppm level H_2S gas at room temperature. Sens Actuator B Chem 120(1):316–323
118. Khanna A, Kumar R, Bhatti SS (2003) CuO-doped SnO_2 thin films as hydrogen sulfide gas sensor. Appl Phys Lett 82:4388. https://doi.org/10.1063/1.1584071
119. Tao W-H, Tsai C-H (2002) H_2S sensing properties of noble metal-doped WO_3 thin film sensor fabricated by micromachining. Sens Actuator B 81(2–3):237–247. https://doi.org/10.1016/S0925-4005(01)00958-3
120. Chaudhari GN, Bambole DR, Bodade AB, Padol PR (2006) Characterization of nanosized TiO_2 based H_2S gas sensor. J Mater Sci 41(15):4860–4864. https://doi.org/10.1007/s10853-006-0042-7
121. Li Z, Huang Y, Zhang S, Chen W, Kuang Z, Ao D (2015) A fast response and recovery H_2S gas sensor based on α-Fe_2O_3 nanoparticles with ppb level detection limit. J Hazard Mater 300:167–174. https://doi.org/10.1016/j.jhazmat.2015.07.003
122. Gopal Reddy CV, Manorama SV, Rao VJ (2000) Preparation and characterization of ferrites as gas sensor materials. J Mater Sci Lett 19(9):775–778. https://doi.org/10.1023/A:1006716721984
123. Haija MA, Abu Hani AFS, Hamdan N, Stephen S (2017) Characterization of H_2S gas sensor based on $CuFe_2O_4$ nanoparticles. J Alloys Compd 690(5):461–468. https://doi.org/10.1016/j.jallcom.2016.08.174
124. Moon S, Vuong NM, Lee D, Kim D, Lee H, Kim D (2016) Co_3O_4–SWCNT composites for H_2S gas sensor application. Sens Actuator B 222:166–172. https://doi.org/10.1016/j.snb.2015.08.072
125. Gu H, Wang Z, Hu Y (2012) Hydrogen gas sensors based on semiconductor oxide nanostructures. Sensors 12(5):5517–5550. https://doi.org/10.3390/s120505517
126. Samerjai T, Tamaekong N, Liewhiran C, Wisitsoraat A, Tuantranont A, Phanichphant S (2011) Selectivity towards H_2 gas by flame-made Pt loaded WO_3 sensing films. Sens Actuator B 157:290–297. https://doi.org/10.1016/j.snb.2011.03.065
127. Boudiba A, Zhang C, Umek P, Bittencourt C, Snyders R, Oliver MG (2013) Sensitive and rapid hydrogen sensors based on Pd-WO_3, thick films with different morphologies. Int J Hydrog Energy 38:2565–2577. https://doi.org/10.1016/j.ijhydene.2012.11.040
128. Hucka R, Böttgera U, Kohla D, Heilanda G (1989) Spillover effects in the detection of H_2 and CH_4 by sputtered SnO_2 films with Pd and PdO deposits. Sens Actuator B 17:355–359
129. Samerjai T, Tamaekong N, Liewhiran C, Wisitsoraat A, Tuantranont A, Phanichphant S (2011) Selectivity towards H_2 gas by flame-made Pt loaded WO_3 sensing films. Sens Actuator B 157:290–297. https://doi.org/10.1016/j.snb.2011.03.065
130. Tamaekong N, Liewhiran C, Wisitsoraat A, Phanichphant S (2011) Acetylene sensor based on Pt/ZnO thick films as prepared by flame spray pyrolysis. Sens Actuator B 152:155–161. https://doi.org/10.1016/j.snb.2010.11.058
131. Tan J, Wlodarski W, Kalantar-Zadeh K (2007) Nitrogen dioxide gas sensors based on titanium dioxide thin films deposited on langasite. Thin Solid Films 515:8738–8743. https://doi.org/10.1016/j.tsf.2007.04.008
132. Alsaif MMYA, Balendhran S, Field MR, Latham K, Wlodarski W, Ou JZ, Kalantar-Zadeh K (2014) Two dimensional, MoO_3 nanoflakes obtained using solvent assisted grinding and sonication method: application for H_2 gas sensing. Sens Actuators B 192:196–204. https://doi.org/10.1016/j.snb.2013.10.107
133. Rani RA, Zoolfakar AS, Ou JZ, Field MR, Austin M, Kalantar-Zadeh K (2013) Nanoporous Nb_2O_5 hydrogen gas sensor. Sens Actuator B 176:149–156. https://doi.org/10.1016/j.snb.2012.09.028
134. Mondal B, Basumatari B, Das J (2014) ZnO–SnO_2 based composite type gas sensor for selective hydrogen sensing. Sens Actuator B 194:389–396. https://doi.org/10.1016/j.snb.2013.12.093
135. Zhang D, Sun Y, Jiang C, Zhang Y (2017) Room temperature hydrogen gas sensor based on palladium decorated tin oxide/molybdenum disulfide ternary hybrid via hydrothermal route. Sens Actuator B 242:15–24. https://doi.org/10.1016/j.snb.2016.11.005
136. Korotcenkov G, Cho BK (2017) Metal oxide composites in conductometric gas sensors: achievements and challenges. Sens Actuator B 244:182–210. https://doi.org/10.1016/j.snb.2016.12.117
137. Liu X, Chen C, Zhao Y, Jia BA (2013) Review on the synthesis of manganese oxide nanomaterials and their applications on lithium-ion batteries. J Nanomater. 736375, 1–7. https://doi.org/10.1155/2013/736375
138. Jeong YU, Manthiram A (2002) Nanocrystalline manganese oxides for electrochemical capacitors with neutral electrolytes. J Electrochem Soc 149(11):A1419–A1422. https://doi.org/10.1149/1.1511188
139. Sun Y, Hu X, Luo W, Huang Y (2012) Porous carbon-modified MnO disks prepared by a microwave-polyol process and their superior lithium-ion storage properties. J Mater Chem 22:19190. https://doi.org/10.1039/C2JM32036C
140. Xiao W, Chen JS, Lu Q, Lou XW (2010) Porous spheres assembled from polythiophene (PTh)-coated ultrathin MnO_2 nanosheets with enhanced lithium storage capabilities. J Phys Chem C 114(27):12048–12051. https://doi.org/10.1021/jp104227e
141. Zheng M, Tang H, Li L, Hu Q, Zhang L, Xue H, Pang H (2018) Review hierarchically nanostructured transition metal oxides for lithiumion batteries. Adv Sci 5(3):1–24. https://doi.org/10.1002/advs.201700592
142. Li WY, Xu LN (2005) Co_3O_4 nanomaterials in lithium-ion batteries and gas sensors. J Chem Adv Funct Mater 15(5):851–857. https://doi.org/10.1002/adfm.200400429
143. Su H, Jaffer S, Yu H (2016) Transition metal oxides for sodium-ion batteries. Energy Storage Mater 5:116–131. https://doi.org/10.1016/j.ensm.2016.06.005
144. Wang L, Wei Z, Mao M, Wang H, Ma J (2019) Metal oxide/graphene composite anode materials for sodium-ion batteries. Energy Storage Mater 16:434–454. https://doi.org/10.1016/j.ensm.2018.06.027
145. Wu Z-S, Zhou G, Yin L-C, Ren W, Li F, Cheng H-M (2012) Review-Graphene/metal oxide composite electrode materials for energy storage. Nano Energy 1(1):107–131. https://doi.org/10.1016/j.nanoen.2011.11.001

146. Miracle DB, Senkov ON (2017) A critical review of high entropy alloys and related concepts. Acta Mater 122:448–511. https://doi.org/10.1016/j.actamat.2016.08.081
147. Rost CM, Sachet E, Borman T, Mionsoballegh A, Dickey EC, Hou D, Jones JL, Curtarolo S, Maria J-P (2015) Entropy-stabilized oxides. Nat Commun 6:8485. https://doi.org/10.1038/ncomms9485
148. Bérardan D, Franger S, Dragoe D, Meena AK, Dragoe N (2016) Colossal dielectric constant in high entropy oxides. Phys Status Solidi Rapid Res Lett 10:328–333. https://doi.org/10.1002/pssr.201600043
149. Bérardan D, Franger S, Meena AK, Dragoe N (2016) Room temperature lithium superionic conductivity in high entropy oxides. J Mater Chem A 4:9536–9541. https://doi.org/10.1039/C6TA03249D
150. Sarkar A, Djenadic R, Usharani NJ, Sanghvi KP, Chakravadhanula VSK, Gandhi AS, Hahn H, Bhattacharya SS (2017) Nanocrystalline multicomponent entropy stabilised transition metal oxides. J Eur Ceram Soc 37(2):747–754. https://doi.org/10.1016/j.jeurceramsoc.2016.09.018
151. Sarkar A, Velasco L, Wang D, Wang Q, Talasila G, de Biasi L, Kübel C, Brezesinski T, Bhattacharya SS, Hahn H, Breitung B (2018) High entropy oxides for reversible energy storage. Nat Commun 9:3400. https://doi.org/10.1038/s41467-018-05774-5
152. Jose R, Thavasi V, Ramakrishna S (2009) Metal oxides for dye-sensitized solar cells. J Am Ceram Soc 92(2):289–301. https://doi.org/10.1111/j.1551-2916.2008.02870.x
153. Anderson AY, Bouhadana Y, Barad H-N, Kupfer B, Rosh-Hodesh E, Aviv H, Tischler YR, Rühle S, Zaban A (2014) Quantum efficiency and bandgap analysis for combinatorial photovoltaics: sorting activity of Cu-O compounds in all-oxide device libraries. ACS Comb Sci 16(2):53–65. https://doi.org/10.1021/co3001583
154. Sullivan I, Zoellner B, Maggard PA (2016) Copper (I)-based p-type oxides for photoelectrochemical and photovoltaic solar energy conversion. Chem Mater 28(17):5999–6016. https://doi.org/10.1021/acs.chemmater.6b00926
155. Georgieva V, Tanusevski A, Georgieva M (2011) In: Kosyachenko LA (ed) Low-cost solar cells based on cuprous oxide, solar cells-thin-film technologies. InTech. ISBN: 978-953-307-570-9. https://www.intechopen.com/books/solar-cells-thin-film-technologies/low-cost-solar-cells-based-on-cuprous-oxide. Accessed Feb 2019
156. Mittiga A, Salza E, Sarto F, Tucci M, Vasanthi R (2006) Heterojunction solar cell with 2% efficiency based on a Cu_2O substrate. Appl Phys Lett 88:163502–1–163502-2. https://doi.org/10.1063/1.2194315
157. Olsen LC, Addis FW, Miller W (1982) Experimental and theoretical studies of Cu_2O solar cells. Sol Cells 7(3):247–279
158. McShane CM, Choi KS (2012) Junction studies on electrochemically fabricated p–n Cu_2O homojunction solar cells for efficiency enhancement. Phys Chem Chem Phys 14:6112–6118. https://doi.org/10.1039/c2cp40502d
159. Wijesundera RP, Gunawardhana LKADDS, Siripala W (2016) Electrodeposited Cu_2O homojunction solar cells: fabrication of a cell of high short circuit photocurrent. Sol Energy Mater Solar Cells 157:881–886. https://doi.org/10.1016/j.solmat.2016.07.005
160. Han K, Tao M (2009) Electrochemically deposited p–n homojunction cuprous oxide solar cells. Sol Energy Mater Sol Cells 93(1):153–157. https://doi.org/10.1016/j.solmat.2008.09.023
161. Minami T, Miyata T, Nishi Y (2016) The relationship between the electrical properties of the n-oxide and p-Cu_2O layers and the photovoltaic properties of Cu_2O-based heterojunction solar cells. Sol Energy Mater Sol Cells 147:85–93. https://doi.org/10.1016/j.solmat.2015.11.033
162. Chen X, Lin P, Yan X, Bai Z, Yuan H, Shen Y, Liu Y, Zhang G, Zhang Z, Zhang Y (2015) Three-dimensional ordered ZnO/Cu_2O nanoheterojunctions for efficient metal–oxide solar cells. ACS Appl Mater Interfaces 7(5):3216–3223. https://doi.org/10.1021/am507836v
163. Anderson J, Van de Walle CG (2009) Fundamentals of zinc oxide as a semiconductor. Rep Prog Phys 72(12):126501. https://doi.org/10.1088/0034-4885/72/12/126501
164. Siddiqui H, Parra MR, Pandey P, Singh N, Qureshi, Haque FZ (2012) A review: synthesis, characterization and cell performance of Cu_2O based material for solar cells. Orient J Chem 28(3):1533–1545
165. Lee YS, Chua D, Brandt RE, Siah SC, Li JV, Mailoa JP, Lee SW, Gordon RG, Buonassisi T (2014) Atomic layer deposited gallium oxide buffer layer enables 1.2 V open-circuit voltage in cuprous oxide solar cells. Adv Mater 26(27):4704–4710. https://doi.org/10.1002/adma.201401054
166. Musselman KP, Wisnet A, Iza DC, Hesse HC, Scheu C, MacManus-Driscoll JL, Schmidt-Mende L (2010) Strong efficiency improvements in ultra-low-cost inorganic nanowire solar cells. Adv Mater. https://doi.org/10.1002/adma.201090115
167. Patel M, Kim H-S, Kim J, Yun J-H, Kim SJ, Choi EH, Park H-H (2017) Excitonic metal oxide heterojunction (NiO/ZnO) solar cells for all-transparent module integration. Sol Energy Mater Sol Cells 170:246–253. https://doi.org/10.1016/j.solmat.2017.06.006
168. Rühle S, Anderson AY, Barad H-N, Kupfer B, Bouhadana Y, Rosh-Hodesh E, Zaban A (2012) All-oxide photovoltaics. J Phys Chem Lett 3(24):3755–3764. https://doi.org/10.1021/jz3017039
169. Yang XL, Su XD, Shen MR, Zheng FG, Xin Y, Zhang L, Hua MC, Chen YJ, Harris VG (2012) Enhancement of photocurrent in ferroelectric films via the incorporation of narrow bandgap nanoparticles. Adv Mater 24:1202–1208. https://doi.org/10.1002/adma.201104078
170. Dharmadhikari VS, Grannemann WW (1982) Photovoltaic properties of ferroelectric $BaTiO_3$ thin films RF sputter deposited on silicon. J Appl Phys 53(12):8988–8992
171. Suzuki N, Osada M, Billah M, Bando Y, Yamauchi Y, Hossain SA (2018) Chemical synthesis of porous barium titanate thin film and thermal stabilization of ferroelectric phase by porosity-induced strain. J Vis Exp 13:e57441. https://doi.org/10.3791/57441
172. Jiang W, Cai W, Lin Z, Fu C (2013) Effects of Nd-doping on optical and photovoltaic properties of barium titanate thin films prepared by sol–gel method. Mater Res Bull 48(9):3092–3097. https://doi.org/10.1016/j.materresbull.2013.04.048
173. Steuber F, Staudigel J, Stossel M, Simmerer J, Winnacker A (1999) Reduced operating voltage of organic electroluminescent devices by plasma treatment of the indium tin oxide anode. Appl Phys Lett 74:3558. https://doi.org/10.1063/1.124160
174. Ali K, Khan SA, Jafri MZM (2014) Structural and optical properties of ITO/TiO_2 anti-reflective films for solar cell applications. Nanoscale Res Lett 9:175. https://doi.org/10.1186/1556-276X-9-175
175. Hrostea L, Boclinca M, Socol M, Leontie L, Stanculescu A, Girtan M (2017) Oxide/metal/oxide electrodes for solar cell applications. Sol Energy 146:464–469. https://doi.org/10.1016/j.solener.2017.03.017
176. Kim D-H, Park M-R, Lee H-J, Lee G-H (2006) Thickness dependence of electrical properties of ITO film deposited on a plastic substrate by RF magnetron sputtering. Appl Surf Sci 253(2):409–411. https://doi.org/10.1016/j.apsusc.2005.12.097
177. Huang Z, He M, Yu M, Click K, Beauchamp D, Wu Y (2015) Dye-controlled interfacial electron transfer for high-current indium tin oxide photocathodes. Angew Chem Int Ed 54:6857–6861. https://doi.org/10.1002/anie.201500274

178. Susarova DK, Akkuratov AV, Kukharenko AI, Cholakh SO, Kurmaev EZ, Troshin PA (2017) ITO modification for efficient inverted organic solar cells. Langmuir 33(39):10118–10124. https://doi.org/10.1021/acs.langmuir.7b01106
179. Kim H, Gilmore C, Pique A, Horwitz J, Mattoussi H, Murata H, Kafafi Z, Chrisey D (1999) Electrical, optical, and structural properties of indium–tin–oxide thin films for organic light-emitting devices. J Appl Phys 86(11):6451–6461. https://doi.org/10.1063/1.371708
180. Kim JH, Kang TW, Kwon SN, Na S-I, Yoo YZ, Im H-S, Seong T-Y (2017) Transparent conductive ITO/Ag/ITO electrode deposited at room temperature for organic solar cells. J Electron Mater 46:306. https://doi.org/10.1007/s11664-016-4956-9
181. Girtan M (2012) Comparison of ITO/metal/ITO and ZnO/metal/ZnO characteristics as transparent electrodes for third generation solar cells. Sol Energy Mater Sol Cells 100:153–161. https://doi.org/10.1016/j.solmat.2012.01.007
182. Ito N, Sato Y, Song PK, Kaijio A, Inoue K, Shigesato Y (2006) Electrical and optical properties of amorphous indium zinc oxide films. Thin Solid Films 496(1):99–103. https://doi.org/10.1016/j.tsf.2005.08.257
183. Kang JW, Jeong WI, Kim JJ, Kim HK, Kim DG, Lee GH (2007) High-performance flexible organic light-emitting diodes using amorphous indium zinc oxide anode. Electrochem Solid State Lett 10(6):J75–J78. https://doi.org/10.1149/1.2720635
184. Warasawa M, Kaijo A, Sugiyama M (2012) Advantages of using amorphous indium zinc oxide films for window layer in Cu(In, Ga)Se_2 solar cells. Thin Solid Films 520(6):2119–2122. https://doi.org/10.1016/j.tsf.2011.08.093
185. Socol G, Craciun D, Mihailescu IN, Stefan N, Besleaga C, Ion L, Antohe S, Kim KW, Norton D, Pearton SJ, Galca AC, Craciun V (2011) High quality amorphous indium zinc oxide thin films synthesized by pulsed laser deposition. Thin Solid Films 520(4):1274–1277. https://doi.org/10.1016/j.tsf.2011.04.196
186. Sheng J, Lee H-J, Oh S, Park J-S (2016) Flexible and high-performance amorphous indium zinc oxide thin-film transistor using low-temperature atomic layer deposition. ACS Appl Mater Interfaces 8(49):33821–33828. https://doi.org/10.1021/acsami.6b11774
187. Naik GV, Shalaev VM, Boltasseva A (2013) Alternative plasmonic materials: beyond gold and silver. Adv Mater 25:3264–3294. https://doi.org/10.1002/adma.201205076
188. Gerischer H, Michel-Beyerle ME, Rebentrost F, Tributsch H (1968) Sensitization of charge injection into semiconductors with large band gap. Electrochim Acta 13(6):1509–1515
189. Yu Z, Perera IR, Daeneke T, Makuta S, Tachibana Y, Jasieniak JJ, Mishra A, Bäuerle P, Spiccia L, Bach U (2016) Indium tin oxide as a semiconductor material in efficient p-type dye-sensitized solar cells. NPG Asia Mater 8:e305. https://doi.org/10.1038/am.2016.89
190. McCune M, Zhang W, Deng Y (2012) High-efficiency dye-sensitized solar cells based on three-dimensional multilayered zno nanowire arrays with "caterpillar-like" structure. Nano Lett 12(7):3656–3662. https://doi.org/10.1021/nl301407b
191. Xu C, Wu J, Desai UV, Gao D (2012) High-efficiency solid-state dye-sensitized solar cells based on TiO_2-coated ZnO nanowire arrays. Nano Lett 12(5):2420–2424. https://doi.org/10.1021/nl3004144
192. Yue W, Wu F, Liu C, Qiu Z, Cui Q, Zhang H, Gao F, Shen W, Qiao Q, Wang M (2013) Incorporating $CuInS_2$ quantum dots into polymer/oxide-nanoarray system for efficient hybrid solar cells. Sol Energy Mater Sol Cells 114:43–53. https://doi.org/10.1016/j.solmat.2013.02.021
193. Wang M, Bai S, Chen A, Duan Y, Liu Q, Li D, Lin Y (2012) Improved photovoltaic performance of dye-sensitized solar cells by Sb-doped TiO_2 photoanode. Electrochim Acta 77:54–59. https://doi.org/10.1016/j.electacta.2012.05.050
194. Cao J, Ertekin E, Srinivasan V, Fan W, Huang S (2009) Strain engineering and one-dimensional organization of metal-insulator domains in single-crystal vanadium dioxide beams. Nat Nanotechnol 4:732–737. https://doi.org/10.1038/nnano.2009.266
195. Liu M, Hwang HY, Tao H, Strikwerda AC, Fan K, Keiser GR, Sternbach AJ, West KG, Kittiwatanakul S, Lu J et al (2012) Terahertz-field-induced insulator-to-metal transition in vanadium dioxide metamaterial. Nature 487:345–348. https://doi.org/10.1038/nature11231
196. Patent application 20090022977, US Patent 7,704,553; NASA Disclosures LAR-17638-1 and LAR-17427-1. https://www.techbriefs.com/dl/HOT100/DielecMats.pdf. Accessed Aug 2018
197. Saini A, Kumar P, Ravelo B, Thakur A, Thakur P (2016) Dielectric parameter estimation of novel magneto-dielectric substrate based microstrip antenna. IP Conf Proc 1731:060021. https://doi.org/10.1063/1.4947827
198. Wassei JK, Kaner RB (2010) Graphene, a promising transparent conductor. Mater Today 13:52–59. https://doi.org/10.1016/S1369-7021(10)70034-1
199. Varghese OK, Paulose M, Grimes CA (2009) Long vertically aligned titania nanotubes on transparent conducting oxide for highly efficient solar cells. Nat Nanotechnol 4:592–597. https://doi.org/10.1038/nnano.2009.226
200. Hautcoeur J, Colombel F, Castel X, Himdi M, Motta Cruz E (2009) Optically transparent monopole antenna with high radiation efficiency manufactured with silver grid layer (AgGL). Electron Lett 45:1014–1016. https://doi.org/10.1049/el.2009.1218
201. Moharram MA, Kishk AA (2016) Optically transparent reflectarray antenna design integrated with solar cells. IEEE Trans Antennas Propag 64(5):1700–1712. https://doi.org/10.1109/TAP.2016.2539379
202. Dao QH, Cherogony TJ, Geck B (2016) Optically transparent and circularly polarized patch antenna for K-band applications. In: Proceedings of German microwave conference GeMiC, pp 247–250. https://doi.org/10.1109/gemic.2016.7461602
203. Anand S, Kumar DS, Wu RJ, Chavali M (2014) Analysis and design of optically transparent antenna on photonic band gap structures. Optik 125:2835–2839. https://doi.org/10.1016/j.ijleo.2013.11.061
204. Anand S, Sudesh DM, Kumar DS, Murthy C (2015) Analysis of titanium-doped indium oxide based optically transparent patch antenna for terahertz communications. J Comput Theor Nanosci 12(3):341–344
205. Anand S, Darak MS, Kumar DS (2014) Investigation of fluorine-doped tin oxide based optically transparent E-shaped patch antenna for terahertz communications. AIP Conf Proc 1620:430. https://doi.org/10.1063/1.4898277
206. Colombel F, Castel X, Himdi M, Legeay G, Vigneron S, Cruz EM (2009) Ultrathin metal layer, ITO film and ITO/Cu/ITO multilayer towards the transparent antenna. IET Sci Meas Technol 3:229–234. https://doi.org/10.1049/iet-smt:20080060
207. Sailing H, Yanxi C, Yuqian Y, Pu Z, Yi J (2009) Review: Optical nano-antennas and metamaterials. Mater Today 12:16–24. https://doi.org/10.1016/S1369-7021(09)70313-X
208. Yao Y, He N, Chen W, Yu J, Chen X (2015) Novel optically transparent antenna for RFID smart fitting room application. In: Proceedings of Asia-Pacific microwave conference APMC, pp 1–3
209. Exarhos GJ, Zhou X-D (2007) Discovery-based design of transparent conducting oxide films. Thin Solid Films 515(18):7025–7052. https://doi.org/10.1016/j.tsf.2007.03.014
210. Rani MSA, Rahim SKA, Kamarudin MR, Peter T, Cheung SW, Saad BM (2014) Electromagnetic behaviours of thin film CPW-Fed CSRR loaded on UWB transparent antenna. IEEE Antennas

Wirel Propag Lett 13:1239–1242. https://doi.org/10.1109/LAWP.2014.2332514
211. Mias C (2000) Optically transparent microstrip antennas. In: Proceedings of IEE colloquium on antennas for automotives. London, p 8
212. Hautcoeur J, Colombel F, Castel X, Himdi M, Motta-Cruz E (2011) Radiofrequency performances of transparent ultra-wideband antennas. Prog Electromagn Res C 22:259–271. https://doi.org/10.2528/PIERC11052606
213. Guan N, Furuya H, Hosono R, Tayama H, Yamagami K (2012) A see-through wire-grid film antenna for WLAN applications. In: Proceedings of IEEE Asia-Pacific conference on antennas and propagation, APCAP, pp 273–274
214. Lim EH, Leung KW (2010) Transparent dielectric resonator antennas for optical applications. IEEE Trans Antennas Propag 58:1054–1059. https://doi.org/10.1109/TAP.2010.2041315
215. Lin Y, Watson KA, Fallbach MJ, Ghose S, Smith JG Jr, Delozier DM, Cao W, Crooks RE, Connell JW (2009) Rapid, solventless, bulk preparation of metal nanoparticle-decorated carbon nanotubes. ACS Nano 3(4):871–884
216. Dezern K (2015) Tailored dielectric materials with metal and metal oxide nanoparticles. Electronics. https://contest.techbriefs.com/2015/entries/electronics/5704-tailored-dielectric-materials-with-metal-and-metal-oxide-nanoparticles
217. Donchev E, Pang JS, Gammon PM, Centeno A, Xie F, Petrov PK, Breeze JD, Ryan MP, Riley DJ, Alford McNN (2014) The rectenna device: from theory to practice (a review). MRS Energy Sustain Rev J 1:1–34. https://doi.org/10.1557/mre.2014.6
218. Parretta A, Jayaraj MK, Di Nocera A, Loreti S, Quercia L, Agati A (1996) Electrical and optical properties of copper oxide films prepared by reactive RF magnetron sputtering. Phys Status Solidi 155:399–404. https://doi.org/10.1002/pssa.2211550213
219. Grover S, Moddel G (2012) Engineering the current-voltage characteristics of metal-insulator-metal diodes using double-insulator barriers. Solid State Electron 67:94–99. https://doi.org/10.1016/j.sse.2011.09.004
220. Banerjee AN, Kundoo S, Saha P, Chattopadhyay KK (2003) Synthesis and characterization of nano-crystalline fluorine-doped SnO_2 thin films by sol–gel method. J Sol–Gel Sci Technol 28:105–110. https://doi.org/10.1023/A:1025697322395
221. Banerjee AN, Maity R, Kundoo S, Chattopadhyay KK (2004) Poole-Frenkel effect in nanocrystalline SnO_2: F thin films prepared by sol–gel-dip-coating technique. Phys Stat Solid A 201:983–989. https://doi.org/10.1002/pssa.200306766
222. Zhang KHL, Xi K, Blamire MG, Egdell RG (2016) P-type transparent conducting oxides. J Phys Condens Matter 28:383002. https://doi.org/10.1088/0953-8984/28/38/383002
223. Wei S-H, Nie X, Zhang SB (2002) Electronic structure and doping of p-type transparent conducting oxides. In: Proceedings of twenty-ninth IEEE photovoltaic specialists conference. INSPEC Accession Number: 7755119. https://doi.org/10.1109/pvsc.2002.1190610
224. Hu L, Wei R, Yan J, Wang D, Tang X, Luo X, Song W, Dai J, Zhu X, Zhang C, Sun Y (2018) La2/3Sr1/3VO_3 thin films: a new p-type transparent conducting oxide with very high figure of merit. Adv Electron Mater 4(3):1700476. https://doi.org/10.1002/aelm.20170047